


# Derivation of consistent hard rock ( $1000 < V_S < 3000$ m/s) GMPEs from surface and down-hole recordings: analysis of KiK-net data

A. Laurendeau<sup>1,2</sup>  · P.-Y. Bard<sup>3</sup> · F. Hollender<sup>3,4</sup> ·  
V. Perron<sup>4</sup> · L. Foundotos<sup>4</sup> · O.-J. Ktenidou<sup>5</sup> ·  
B. Hernandez<sup>1</sup>

Received: 15 October 2016 / Accepted: 19 April 2017  
© The Author(s) 2017. This article is an open access publication

**Abstract** A key component in seismic hazard assessment is the estimation of ground motion for hard rock sites, either for applications to installations built on this site category, or as an input motion for site response computation. Empirical ground motion prediction equations (GMPEs) are the traditional basis for estimating ground motion while  $V_{S30}$  is the basis to account for site conditions. As current GMPEs are poorly constrained for  $V_{S30}$  larger than 1000 m/s, the presently used approach for estimating hazard on hard rock sites consists of “host-to-target” adjustment techniques based on  $V_{S30}$  and  $\kappa_0$  values. The present study investigates alternative methods on the basis of a KiK-net dataset corresponding to stiff and rocky sites with  $500 < V_{S30} < 1350$  m/s. The existence of sensor pairs (one at the surface and one in depth) and the availability of P- and S-wave velocity profiles allow deriving two “virtual” datasets associated to outcropping hard rock sites with  $V_S$  in the range [1000, 3000] m/s with two independent corrections: 1/down-hole recordings modified from within motion to outcropping motion with a depth correction factor, 2/surface recordings deconvolved from their specific site response derived through 1D simulation. GMPEs with simple functional forms are then developed, including a  $V_{S30}$

---

The following softwares are employed in this study: 1) the one written by J.-C. Gariel and P.-Y. Bard of the 1D reflectivity approach (Kennett 1974); 2) the `site_amp` v.5.6 program package provided by Dave Boore (U.S. Geological Survey); and the `pikwin` software developed by Perron et al. (2017).

---

✉ A. Laurendeau  
aurore.laurendeau@gmail.com

O.-J. Ktenidou  
o.ktenidou@gre.ac.uk

<sup>1</sup> CEA, DAM, DIF, 91297 Arpajon, France

<sup>2</sup> Present Address: Instituto Geofísico Escuela Politécnica Nacional, Quito, Ecuador

<sup>3</sup> ISTerre, University of Grenoble Alpes/IFSTTAR, CS 40700, 38058 Grenoble, France

<sup>4</sup> CEA, DEN, 13108 St. Paul lez Durance Cedex, France

<sup>5</sup> Department of Engineering Science, University of Greenwich, Central Avenue, Chatham Maritime, Kent ME4 4TB, UK

site term. They lead to consistent and robust hard-rock motion estimates, which prove to be significantly lower than host-to-target adjustment predictions. The difference can reach a factor up to 3–4 beyond 5 Hz for very hard-rock, but decreases for decreasing frequency until vanishing below 2 Hz.

**Keywords** Hard rock reference motion · Site effects · KiK-net · GMPE · “Host-to-target” adjustments

## 1 Introduction

Site-specific seismic hazard analysis (SHA) often requires the assessment of regional hazard for very hard-rock conditions. The presently available methods are all based on the concept of “host-to-target” adjustment (H2T), with different implementations (e.g., Campbell 2003; Al Atik et al. 2014) which all imply a number of underlying assumptions. The objective of the present paper is to investigate some new approaches to develop ground motion prediction equation (GMPE) which be valid for hard rock sites characterized by  $V_{S30} \geq 1500$  m/s, and to compare their outcomes with more classical H2T approach.

To assess regional seismic hazard in areas of low-to-moderate seismicity (classically called target region), we typically use GMPEs derived with seismic records from surface stations located in active seismic areas (host region). These GMPEs are in most cases developed by mixing different site conditions, with a majority of soil sites (see Ancheta et al. 2014 for the NGA West 2 database; Akkar et al. 2014 for the RESORCE database). In most GMPEs, the site is described through a single proxy, the average shear wave velocity over the upper 30 m ( $V_{S30}$ ) (e.g., Boore and Atkinson 2008). Several studies have shown the interest to complement this characterization, at least for rock sites, with their high frequency attenuation properties (e.g., Silva et al. 1998; Douglas et al. 2010; Edwards et al. 2011; Chandler et al. 2006). The proxy that is often used in the engineering seismology community to characterize the site-specific high-frequency content of records is the “ $\kappa_0$ ” value, introduced first by Anderson and Hough (1984) to represent the attenuation of seismic waves in the first few hundreds of meters or kilometers beneath the site. Classically,  $\kappa_0$  is obtained after a measurement on several tens of records of the high frequency decay  $\kappa$  of the acceleration Fourier amplitude spectrum (FAS), and investigating its dependence on the epicentral distance  $R$  in a log-linear space, which exhibits a relationship  $\kappa(r) = \kappa_0 + \alpha \cdot \log(R)$ , where the trend coefficient  $\alpha$  is related to the regional  $Q$  attenuation effect (Anderson and Hough 1984). The model is described as:

$$A(f) = A_0 \exp[-\pi\kappa(R)f] \quad \text{for } f > f_E \quad (1)$$

in which  $A(f)$  is FAS,  $A_0$  is a source- and propagation-path-dependent amplitude,  $f_E$  is the frequency above which the decay is approximately linear, and  $R$  is the epicentral distance. A review of the definition and estimation approaches of  $\kappa_0$  is given by Ktenidou et al. (2014). A rock site can be described with these two proxies,  $V_{S30}$  and  $\kappa_0$ , for instance in the stochastic simulation method of Boore (2003). Some recent studies have also shown the usefulness to include the  $\kappa_0$  proxy directly in GMPEs as a complement to  $V_{S30}$  to better estimate the rock motion (Laurendeau et al. 2013; Bora et al. 2015). The  $\kappa_0$  parameter may also be related, at least partly, to the near-surface attenuation characterized by the S-wave quality factor  $Q_S$  (or alternatively the damping  $\zeta$  used in the geotechnical engineering practice, i.e.,  $\zeta = 0.5/Q_S$ ). If the site underground structure (at the scale of a few hundred

meters to a few kilometers) is characterized by a stack of  $N$  horizontal layers with different velocity ( $V_{Si}$ ,  $i = 1, N$ ) and damping ( $Q_{Si}$ ) characteristics, the corresponding site-specific intrinsic attenuation may be integrated along the path of the seismic waves through these  $N$  shallow layers, as indicated by Hough and Anderson (1988):

$$\kappa_0 = \sum_{i=1}^N \frac{h_i}{Q_{Si} V_{Si}} \quad (2)$$

In this case,  $Q_s$  considers only the effect of intrinsic attenuation while  $\kappa_0$  includes also scattering, especially coming from the soft shallow layers (Ktenidou et al. 2015; Pilz and Fäh 2017).

To predict site-specific ground motions (e.g., Rodriguez-Marek et al. 2014; Aristizabal et al. 2016, 2017), the definition of input motion for site response calculations often requires the prediction for a hard-rock site ( $V_{S30} > 1500$  m/s and low  $\kappa_0$  values). However, most of the presently existing GMPEs do not allow such predictions (e.g., Laurendeau et al. 2013). One solution that was adopted in recent PSHA projects [e.g., Probabilistic Seismic Hazard Analysis for Swiss Nuclear Power Plant Sites (PEGASOS)] is to adjust existing GMPEs from the host to the target region, in terms of source, propagation and site conditions (e.g., Campbell 2003; Cotton et al. 2006). These adjustments require a good understanding of the mechanisms controlling the ground motion. However, the source (e.g., stress drop, magnitude scaling) and crustal propagation (e.g., quality factor and its frequency dependence) terms are not well constrained. In recent projects (e.g., PEGASOS Refinement Project, Biro and Renault 2012; Thyspunt Nuclear Siting Project, Rodriguez-Marek et al. 2014), the empirically predicted motion is thus corrected by a theoretical adjustment factor depending only on two site parameters,  $V_{S30}$  and  $\kappa_0$ . For example, the adjustment factor as proposed by Van Houtte et al. (2011) is a ratio of acceleration response spectra obtained from the point source stochastic simulation method of Boore (2003). This ratio is computed, for different ranges of magnitude-distance, between a “standard” rock characterized by a  $V_{S30}$  around 800 m/s and  $\kappa_0$  typically between 0.02 and 0.05 s (characteristics of the host region), and a “hard rock” characterized by larger  $V_{S30}$  values (from 1500 to over 3000 m/s), and different  $\kappa_0$  values, typically lower to much lower. The two site amplifications are assessed with the quarter wavelength method (Joyner et al. 1981; Boore 2003) using a family of generic velocity profiles (Boore and Joyner 1997; Cotton et al. 2006) tuned to  $V_{S30}$  values, and the  $\kappa_0$  effect is then added according to Eq. (1). In such approaches,  $\kappa_0$  is most often derived from empirical  $V_{S30}$ - $\kappa_0$  relationships established with data coming from different studies in the world (Silva et al. 1998; Douglas et al. 2010; Drouet et al. 2010; Edwards et al. 2011; Chandler et al. 2006; Van Houtte et al. 2011). The short overview of such relationships presented in Kottke (2017) indicates typical  $\kappa_0$  values around between 0.02 and 0.05 s for standard rock conditions, and below 0.015 s (and sometimes down to 0.002 s) for hard rock conditions ( $V_{S30} \geq 1500$  m/s). All the corrections are performed in the Fourier domain and then translated in the response spectrum domain using random vibration theory. This procedure—which is thus implicitly based on rather strong assumptions—allows to obtain rather smooth rock site amplification functions. Their ratio is the theoretical adjustment factor: the underlying assumptions indicated above systematically result in a significantly larger high frequency motion on hard rock site compared to softer, “standard” rock sites, due to the much lower attenuation ( $\kappa_0$  effect supersedes impedance effect). The methodology proposed by Van Houtte et al. (2011) is actually not the only way to adjust rock ground motion toward hard-rock motion: Al Atik et al. (2014) propose to estimate the host  $\kappa_0$

directly from the GMPEs through the inverse random vibration theory (IRVT), while Bora et al. (2015) estimate directly the host  $\kappa_0$  values (though not in the classical way) and derive a GMPE in the Fourier domain including it. Both approaches thus allow to avoid the use of  $V_{S30}-\kappa_0$  relationships at least for the host region. However, the latter is presently limited to only one set of data, while the Al Atik et al. (2014) procedure is relatively heavy as the  $\kappa_0$  estimates are scenario dependent. In any case, the comparison recently performed by Ktenidou and Abrahamson (2016) between the adjustment factors obtained with different analytical methods [named IRVT (Al Atik et al. 2014)] and PSSM (point source stochastic method, method similar to Van Houtte et al. 2011), show that for similar ( $V_{S30}$ ,  $\kappa_0$ ) pairs of values, the IRVT method gives the same tendency for the adjustment factor; in particular, hard-rock sites with low  $\kappa_0$  values should undergo larger amplification at high frequency. That is why in this study we have chosen to compare our results only with the PSSM method implemented with the  $V_{S30}-\kappa_0$  relationships proposed by Van Houtte et al. (2011), which can be seen in Kottke (2017) to be a relatively median relation amongst all the data available by the time the present study was finalized (early 2016). It must be mentioned however that the latest results by Ktenidou and Abrahamson (2016) on the NGA-East data conclude at significantly higher than expected  $\kappa_0$  values for hard-rock, eastern NGA sites (typically around 0.02 s), and correlatively smaller motion on hard-rock sites over the whole frequency range, including the high-frequency range where  $\kappa_0$  relationships are expected to be dominant.

In addition, these host-to-target adjustment factors are associated with large epistemic uncertainties, which may greatly impact the resulting ground motions estimates especially for long return periods (e.g., Bommer and Abrahamson 2006). There are mainly three kinds of uncertainties: those associated with the host region, those associated with the target region and those associated with the method to define the adjustment factor. Between the host and the target region, the uncertainties might involve similar issues, addressed however in different ways for the two regions. Generally, on the host side, the  $V_S$ -profile (involving not only  $V_{S30}$ , but also its shape down to several kilometers) and  $\kappa_0$  are at most relatively poorly known, or not constrained at all (e.g., when using a generic velocity profile, or  $\kappa_0$  values derived from statistical  $V_{S30}-\kappa_0$  correlations, ...). On the target side, site-specific hazard assessment studies generally imply site-specific measurements to constrain better the velocity profile and sometimes the  $\kappa_0$  value; in such cases, there however exist residual uncertainties associated with the measurement themselves (especially for  $\kappa_0$  values, see for instance Ktenidou and Abrahamson 2016). As a consequence, a significant source of uncertainties comes from the host GMPE. Indeed, even for a rock with a  $V_{S30}$  of 800 m/s, the prediction is not well constrained, due to (i) a relative lack of records for this category (compared to usual, soft and stiff sites) and (ii) a too simplified site description involving only the  $V_{S30}$  proxy (with often only inferred values) without any precision on the depth profile. Example of such “host-GMPE” uncertainties may be found in Laurendeau et al. (2013) who compared soft-rock to hard-rock ratios for different cases:—empirical ratios from classical, existing GMPEs dependent on only  $V_{S30}$  and developed with a majority of soil sites;—one deduced from a GMPE dependent on only  $V_{S30}$  and developed for sites with  $V_{S30} \geq 500$  m/s;—theoretical ratios dependent on only  $V_{S30}$ ;—and theoretical ratios dependent on  $V_{S30}$  and  $\kappa_0$ . Finally, two main sources of methodological uncertainties may be identified in the approaches presently used to estimate the adjustment factors. First, the rock amplification factor associated to the velocity profile are currently estimated mainly with the impedance, quarter-wavelength approach (QWL) (Boore and Joyner 1997; Boore 2003), which is not able to reproduce the high-frequency amplification peaks often observed on measured surface/downhole transfer

functions for specific rock sites, and interpreted as related to local resonance effects (weathering, fracturing, e.g., Steidl et al. 1996; Cadet et al. 2012). Secondly, the need to move back and forth between Fourier and response spectra through the random vibration theory (RVT and IRVT, see Al Atik et al. 2014; Bora et al. 2015), also introduces some additional uncertainties, as this process is strongly non-linear and non-unique.

To get predictions for sites with higher  $V_{S30}$  ( $\geq 1500$  m/s), another possibility is to employ time-histories recorded at depth. Some GMPEs have been developed from such recordings, especially those of the KiK-net database, which has sensor pairs (e.g., Cotton et al. 2008; Rodriguez-Marek et al. 2011). However, these models are not employed in SHA studies because of the reluctance of many scientists or engineers to use “within-motion”, depth recordings. In addition to the cost of this installation and heterogeneities coming from different depths, these records do not represent neither outcropping motion nor incident motion. They are indeed “within motion” recordings which are affected by destructive interferences between up-going and down-going waves (e.g., Steidl et al. 1996; Bonilla et al. 2002). Therefore, the Fourier spectra shape is modified: a trough appears at the destructive frequency,  $f_{\text{dest}}$ , which is related to the sensor depth (H) and the mean shear wave velocity of the upper layers ( $V_M$ ):  $f_{\text{dest}} = V_M/4H$ . The effects of both destructive interferences and differences of free surface effects have been highlighted by computing the ratio between surface and depth records both from observations and theoretical linear SH-1D simulation. This “outcropping to within motion” ratio is around 1 at frequencies lower than  $0.5 f_{\text{dest}}$ ; at  $f_{\text{dest}}$ , a significant peak is observed due to destructive interferences and finally, at high frequency the ratio is around 1.8 for frequencies exceeding 3 times  $f_{\text{dest}}$ . The difference in amplitude between low and high frequencies is related to free surface effect which is 2 at surface (for quasi-normal incidence) and varying with frequency at the sensor depth. These effects are observable both in the Fourier and the response spectra domains. From these observations, Cadet et al. (2012) have proposed a simplified correction factor for these effects. It was obtained after the analysis of the surface-to-downhole ratios derived on the 5% damping pseudo-acceleration spectra. They chose to work in response spectra domain because its definition implicitly includes a smoothing that limits the effects of destructive interference at depth.

In this study, a specific subset of the KiK-net dataset, corresponding to stiff sites only with  $V_{S30} \geq 500$  m/s, is used: it is the same as in Laurendeau et al. (2013) and the upper limit of  $V_{S30}$  values is 1350 m/s. In a first part, the local site-specific site-responses are estimated with different methods and compared, in order to analyse their reliability in view of their use for deconvolving the surface recordings into hard rock motion. Secondly, alternative methodologies to predict the reference motion are explored. These methods consist in developing GMPEs directly from “virtual” recordings corresponding to outcropping motion at sites with high S-wave velocity. In other words, the objective is to apply site-specific corrections (i.e., methods which generally used only for the target site) to define rock motion in the host region from surface records corrected for the site effects, or from downhole records corrected of the depth effects. From these datasets, simple ground motion prediction equations are developed and the results are compared both with natural data and with classical adjustment method.

## 1.1 The KiK-net dataset

Japan is in an area of high seismicity, where a lot of high quality digital data are made available to the scientific community. The KiK-net network (Okada et al. 2004) offers the advantage of combining pairs of sensors (one at the surface, and one installed at depth in a

borehole), together with geotechnical information. Each instrument is a three-component seismograph with a 24-bit analog-to-digital converter; the KiK-net network uses 200-Hz (until 27 January 2008) and 100-Hz (since 30 October 2007) sampling frequencies. The overall frequency response characteristics of the total system is flat, from 0 to 15 Hz, after which the amplitude starts to decay. The response characteristics are approximately equal to those of a 3-pole Butterworth filter with a cut-off frequency of 30 Hz (Kinoshita 1998; Fujiwara et al. 2004). This filter restricts the analysis to frequencies below 30 Hz.

In the present study, we have used the subset of KiK-net accelerometric data previously built by Laurendeau et al. (2013) consisting basically of crustal events recorded on stiff sites. More precisely, the selection consisted of the following events and sites:

- Events between April 1999 and December 2009,
- Events described in the F-net catalog and for which  $M_{wFnet}$  is larger than 3.5,
- Shallow crustal events with a focal depth less than 25 km were selected and offshore events were excluded,
- Stiff sites for which in surface  $V_{S30} \geq 500$  m/s and at depth  $V_{Shole} \geq 1000$  m/s,
- Surface records with a predicted PGA  $> 2.5$  cm/s<sup>2</sup> using the magnitude-distance filter by Kanno et al. (2006),
- Records with at least 1 s long pre-event noise,
- Following a visual inspection, faulty records, like S-wave triggers, and records including multiple events were eliminated or shortened,
- Events and sites with a minimum of three records satisfying the previous conditions.

Our dataset finally consists of 2086 six-component records, 272 events and 164 sites (Table 1). The magnitude-distance distribution is shown on Fig. 1 (left) (see Laurendeau et al. 2013 for the determination of  $R_{RUP}$ ). The magnitude range is 3.5–6.9 and the rupture distance range is 4–290 km. Figure 1 (right) shows the  $V_S$  distribution of surface and depth records. In surface, there are no sites with  $V_{S30}$  larger than 1500 m/s, and only very few (13) sites with  $V_{S30}$  exceeding 1000 m/s. The down-hole sites allow expanding the distribution until 3000 m/s. The distribution median is around 650 m/s in surface and around 1900 m/s at depth, and around 1100 m/s when surface and down-hole datasets are merged.

**Table 1** Number of records, events and sites for each dataset considered in this study

Datasets	Records	Events	Sites	Mw	SNR	1D condition
Initial	2086	272	164	$\geq 3.5$		
For SSR_dh, HVSR_surf, HVSR_dh	1488	248	152	$\geq 3.5$	$>3$ for the 6 comp. (H and V at surface and depth)	
For DHcor	1031	80	140	$\geq 4.5$	$>3$ for the 2 H comp. at depth	
For SURFcor	765	75	102	$\geq 4.5$	$>3$ for the 2 H comp. at surface	X

The three last columns give information on the criteria used to select the records: the range of magnitude, the signal-to-noise ratio (SNR) threshold which is applied to different components (*H* horizontal, *V* vertical) and the relevancy of the 1D site condition ( $r > 0.6$ ). These different criteria are explained in the corresponding sections describing the various datasets

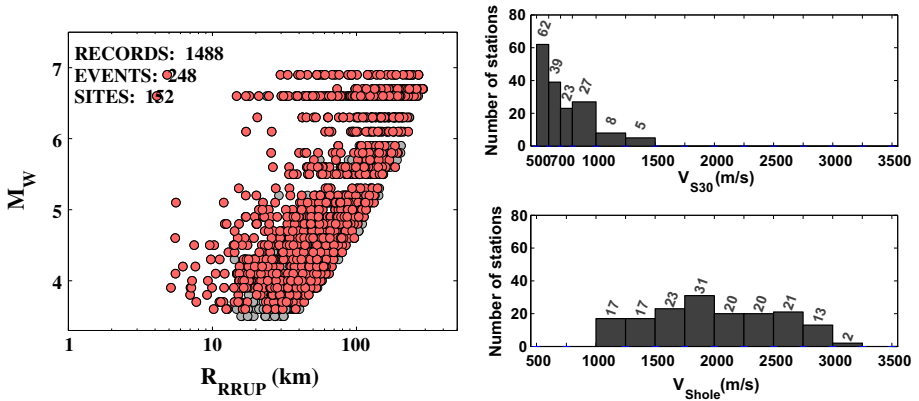


**Fig. 1** *Left* distribution of the moment magnitude ( $M_W$ ) and the rupture distance ( $R_{RRUP}$ ) of the preliminary selection of the KiK-net records (*grey dots*, see Table 1) and then selected to compute the empirical spectral ratios (*red dots*). The records corresponding to the *red dots* have a continuous signal-to-noise ratio larger than 3 between 0.5 and 15 Hz (in this case the signal is the S-wave window). Besides, the empirical spectral ratios are computed for each site and event with at least 3 good records. *Right*  $V_S$  distribution in terms of number of stations: *top* in surface and *bottom* in depth

## 2 Estimation of the site-specific response

A classical way to estimate site effects consists in using spectral ratios of ground motion recordings. The horizontal-to-vertical spectral ratios (HVSr) allow only highlighting  $f_0$  (under some assumptions) that characterize the resonance frequency in presence of strong contrasts (e.g., Lermo and Chavez-Garcia 1993). The standard spectral ratios (SSR, initially proposed by Borchardt 1970) allow quantifying the amplification (Lebrun et al. 2001) with respect to the selected reference. The spectral ratios are computed relative to a site reference chosen either on the surface or on the downhole but near the site, in order that the characteristics of the incident wave field are similar. The choice of the reference site is a sensitive issue (e.g., Steidl et al. 1996).

When records are not available, the linear SH-1D simulation can be used to estimate the theoretical transfer function from the velocity profile. Here, we use the 1D reflectivity model (Kennett 1974) to derive the response of horizontally stratified layers excited by a vertically incident SH plane wave (original software written by Gariel and Bard and used previously in a large number of investigations: e.g., Bard and Gariel 1986; Theodoulidis and Bard 1995; Cadet et al. 2012). This method requires the knowledge of the shear-wave velocity profile [ $V_S(z)$ ]. The other geotechnical parameters are deduced from  $V_S(z)$  using commonly accepted assumptions, the most critical of which deals with quality factor ( $Q_S$ ) values for each layer.

Without information about  $V_S(z)$  but with an idea of  $V_{S30}$ , the amplification of the site can be estimated with the quarter wavelength method (QWL) (e.g., Joyner et al. 1981; Boore 2003) and using generic velocity profiles (Boore and Joyner 1997; Cotton et al. 2006) associated with a  $V_{S30}$  value. This approach is used in most H2T techniques, to compute the adjustment factor, for instance in Van Houtte et al. (2011). It however relies on two strong assumptions: (a)  $V_{S30}$  is considered representative of the whole, deep velocity profile, and (b) the sole impedance effects considered by the QWL method fully

account for the amplification effects on stiff to standard rock sites (in other words, resonance effects are deemed negligible, e.g., Boore 2013).

In this part, the site amplification results obtained from empirical and theoretical methods will be compared and discussed. Figure 2 displays the different measurements in a schematic way.

## 2.1 Computation of the Fourier transfer functions

### 2.1.1 Standard spectral ratios

For each record, the signal-to-noise ratio (SNR) is estimated both for the vertical component and for the 2D complex time-series of the S-wave window of the two orthogonal horizontal time histories as proposed by Tumarkin and Archuleta (1992). Following Kishida et al. (2016), the theoretical S-wave window duration ( $D_S$ ) is defined as a function of source and propagation terms with a minimum duration of 10 s. A noise window is selected before or after the event with a minimum length of 10 s according to a criterion of minimal energy. The windowing and the processing are described in detail in Perron et al. (2017). Each component and window, in surface and at depth, are then processed as following. A first-order baseline operator is applied to the entire record, in order to have a zero-mean of the signal, and a simple baseline correction is applied by removing the linear trend. A 5% cosine taper is applied on each side of the signal window. The records with a 200-Hz sampling frequency are resampled to 100 Hz (to have the same sampling frequency for all the records, without impacting the usable frequency range because of the built-in low-pass filtering around 30 Hz). The records are padded with zeros in order to have the same length for all windows (i.e., 8192 samples). We computed FAS for each component and also for the 2D complex time-series. FAS are smoothed according to the Konno and Ohmachi (1998) procedure with  $b = 30$ . Then, FAS are resampled for a 500 logarithmically spaced sample vector between 0.1 and 50 Hz. Finally, SNR is computed and the record is selected only if SNR is larger than 3 for a continuous frequency band between 0.5 and 15 Hz for both the vertical and horizontal components, both in surface and depth.

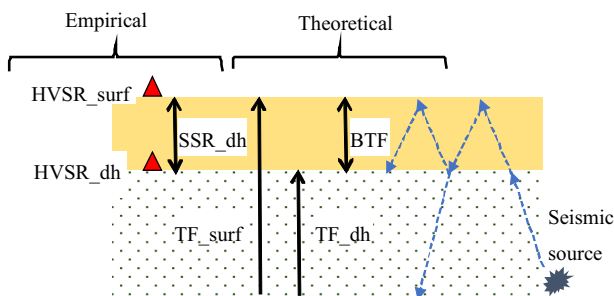


**Fig. 2** Scheme representing the different empirical and theoretical measurements computed to obtain the site amplification for one site. HVSUR is the horizontal-to-vertical spectral ratios (the “\_surf” suffix indicates it is computed at the surface, while the “\_dh” suffix stands for the downhole sensor depth), SSR is the standard spectral ratio (the “\_dh” suffix indicates it is computed with respect to a reference at depth), TF is the numerical transfer function for incident plane S-waves and with respect to outcropping rock (\_surf obtained in surface and \_dh obtained at the sensor depth), BTF is the associated numerical surface to depth transfer function ( $BTF = TF\_surf/TF\_dh$ )



In addition, the geometrical mean of the three empirical spectral ratios (HVSR\_surf, HVSR\_dh, SSR\_dh, see Fig. 2) is estimated if there are at least 3 records for the site. With such selection criteria, the empirical spectral ratios could be finally derived for 152 sites from 1488 records (Fig. 1; Table 1). The most stringent criterion that eliminates most of the  $2086 - 1488 = 598$  recordings is the signal-to-noise threshold.

### 2.1.2 Linear SH-1D simulation

In addition to the velocity profiles [ $V_P(z)$  and  $V_S(z)$ ] derived from downhole measurements, the 1D simulation requires to provide the unit mass [ $\rho(z)$ ] and damping [ $Q_P(z)$  and  $Q_S(z)$ ] profiles. The Brocher (2005) relationship is used to get  $\rho(z)$  from  $V_P(z)$ . The quality factors are assumed to be independent of frequency, and inferred from  $V_S(z)$  according the following relationships:

$$Q_P(z) = \max[V_P(z)/20; V_S(z)/5] \quad (3)$$

and

$$Q_S(z) = V_S(z)/X_Q \quad (4)$$

in which  $X_Q$  is a variable, often chosen equal to 10 (e.g., Fukushima et al. 1995; Olsen et al. 2003; Cadet et al. 2012; Maufroy et al. 2015). Most of the results presented here (unless specifically indicated) correspond to  $X_Q = 10$ ; however, a sensitivity analysis of the impact of  $X_Q$  has been performed to feed the discussion. More details may be found in Hollender et al. (2015).

The numerical transfer functions (TFs) are computed for 2048 frequency samples regularly spaced from 0 to 50 Hz, both at the surface (TF\_surf), and also at the sensor depth TF\_dh. TF\_surf and TF\_dh are computed with respect to an outcropping rock. The Konno and Ohmachi (1998) smoothing is applied with a b coefficient of 10, therefore lower than in the case of real data but theoretical TFs require a stronger smoothing especially at depth because of “pure” destructive interferences (see Cadet et al. 2012). Besides, the theoretical surface to depth transfer function BTF ( $BTF = TF\_surf/TF\_dh$ ) is computed for comparison with the instrumental one SSR\_dh.

## 2.2 Typical site responses

Stiff to “standard-rock” sites present indeed some typical transfer functions which are illustrated and briefly discussed below to highlight some specific features of their behaviour.

Figure 3a presents the example of a site with relatively flat transfer functions, such as what is expected for a reference site, despite the fact this station is characterized by a relatively low  $V_{S30}$ , around 600 m/s. The peak observed on SSR\_dh is interpreted as caused by destructive interferences at depth, since it corresponds to a trough on HVSR\_dh at the same frequency. Would the reference be at the surface, this peak would not exist, as it is the case for HVSR\_surf.

Figure 3b displays an example of a site showing a large amplification, despite the fact that this site, TCGH14, is characterized by a relatively high  $V_{S30}$ , around 850 m/s: this amplification around 10 Hz is larger than 10. In this case, the destructive interference effect is more difficult to observe on SSR but clear on HVSR\_dh: the large amplitude

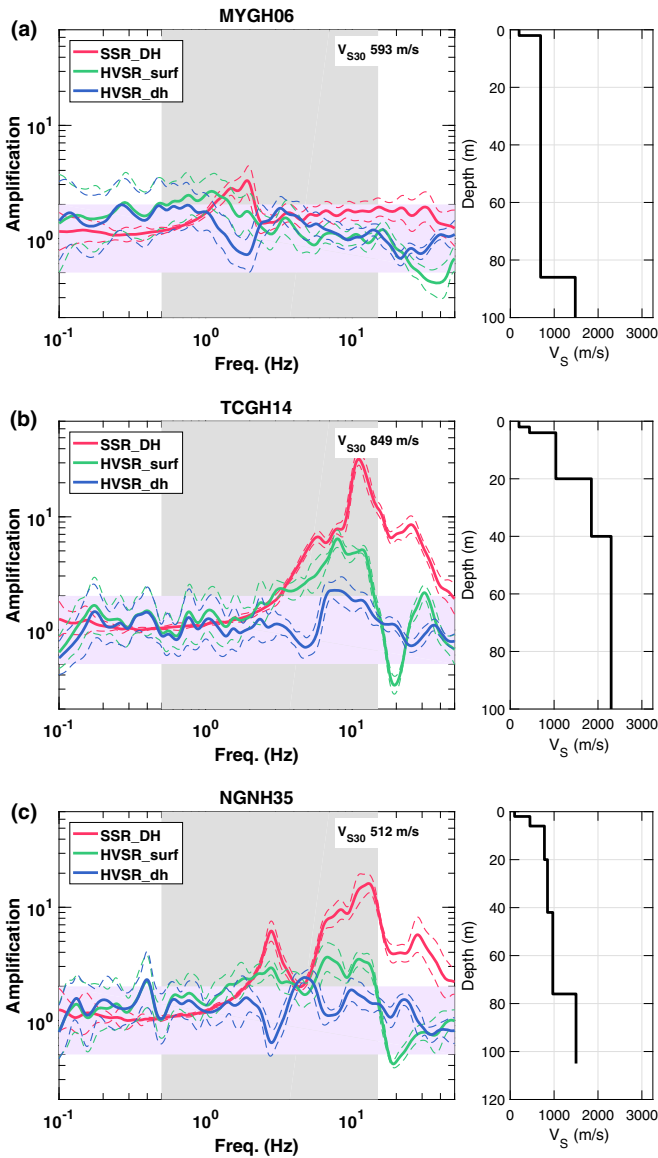


**Fig. 3** Empirical spectral ratios and corresponding S-wave velocity profile for some particular stations. **a** Example of the site MYGH06 which have a relatively flat transfer functions and with a relatively low  $V_{S30}$  (593 m/s). **b** Example of the site TCGH14 showing a large amplification at high frequency with a relatively high  $V_{S30}$  (849 m/s). **c** Example of the site NGNH35 which will be used in the following part as example because it is a well-defined site ( $V_{S30}$  of 512 m/s). The *purple patch* corresponds to amplification levels between 0.5 and 2 and allows to highlight the amplification. The *grey patch* corresponds to the frequency range for which the signal-to-noise-ratio (0.5–15 Hz) is estimated and is higher than 3

(around 10) of the peak at 10 Hz combines the actual surface amplification and the absence of free surface effect at depth for such wavelengths comparable to or smaller than the sensor depth.

Figure 3c shows the example of a well-characterized site (i.e., exhibiting a good correlation coefficient between SSR\_dh and BTF), NGNH35 with a  $V_{S30}$  of 512 m/s. Both HVSR\_surf and SSR\_dh exhibit a first peak around 3 Hz with an amplitude around 2–3 and 5, respectively. As HVSR\_dh exhibits a trough at the same frequency, this first peak is identified as the fundamental frequency of the site, corresponding to a moderate contrast at large depth. The transfer functions present a broad and large amplification from 7 to 12 Hz reaching an amplitude of 16, while the HVSR\_surf also exhibits a peak but with a much more moderate amplitude of 3.5. This high-frequency peak may therefore be interpreted as due to another impedance contrast at shallow depth.

One may notice that the two NGNH35 and TGCH14 are characterized by a large high-frequency amplification (exceeding 10 around 10 Hz), despite having quite different  $V_{S30}$  values. Actually, most of the sites in this KiK-net subset exhibit such a high-frequency amplification (see below).

### 2.3 Comparison of SSR\_dh, BTF and QWL

This part is dedicated to a comparison of the theoretical amplification estimates derived from 1D site response (resonant type BTF, and impedance effects QWL), with the observed SSR\_dh ratios. After a few examples on some typical sites (Fig. 4), this comparison is then performed in a statistical sense on the mean (geometrical average) and standard deviations (natural log) first for all the sites that are likely to be essentially 1D (Fig. 5), and finally for various subsets classified according to their  $V_{S30}$  value (Fig. 6). The downhole-to-surface relative amplification estimate with the QWL approach is computed by using the actual  $V_S(z)$  profile and the  $\Delta\kappa_0$  values corresponding to the cumulative damping effects of each layer from the down-hole sensor to the surface (using Eq. 2 and  $Q_S$  values estimated with Eq. 4).

Such a comparison is indeed acceptable when the site structure is essentially one-dimensional, i.e., with quasi-horizontal layers without significant lateral variations. Thompson et al. (2012) proposed to select 1D sites with reliable velocity profiles by measuring the fit between SSR\_dh and BTF with the Pearson's correlation coefficient ( $r$ ). We implemented the same approach to perform the present statistical comparison:  $r$  has been computed over the frequency range  $[\max(0.5 \text{ Hz}, 0.5 \times f_{\text{dest}}), \min(15 \text{ Hz}, 7 \times f_{\text{dest}})]$ , in which  $f_{\text{dest}}$  is the fundamental frequency of destructive interferences at depth, directly identified on HVSR\_dh (see Fig. 3).

Discrepancies between SSR\_dh and BTF can have at least two origins: (1) the local site geometry is not 1D but 2D or 3D, the 1D simulation is no more applicable or (2) the provided velocity profile of the station is not accurate enough. For Thompson et al. (2012), sites with  $r$  larger than 0.6 are assumed to have 1D-behaviour. Figure 4 shows some examples of sites with good and bad correlation coefficients. NGNH35 exhibits an excellent fit between SSR\_dh and BTF ( $r$  close to 1): BTF predicts the observed amplification in terms of both frequency range and peak amplitude. The slightly lower  $r$  value (0.77) at KYTH02 is associated to the slight over-prediction of the moderate amplitude fundamental peak, while the high-frequency, larger amplification ( $f > 5$  Hz) is very well matched. On the contrary, MYZH05 and NGSH04 are two examples with very low  $r$  values: BTF does not satisfactorily capture either the amplitude and frequency of the large amplitude fundamental peak (NGSH04) or the high frequency amplification (MYZH05).

In our dataset as a whole, a total of 108 sites out of 152, i.e., slightly more than two-thirds, are found to meet the Thompson criterion, i.e.,  $r \geq 0.6$  (see Table 1). In the next

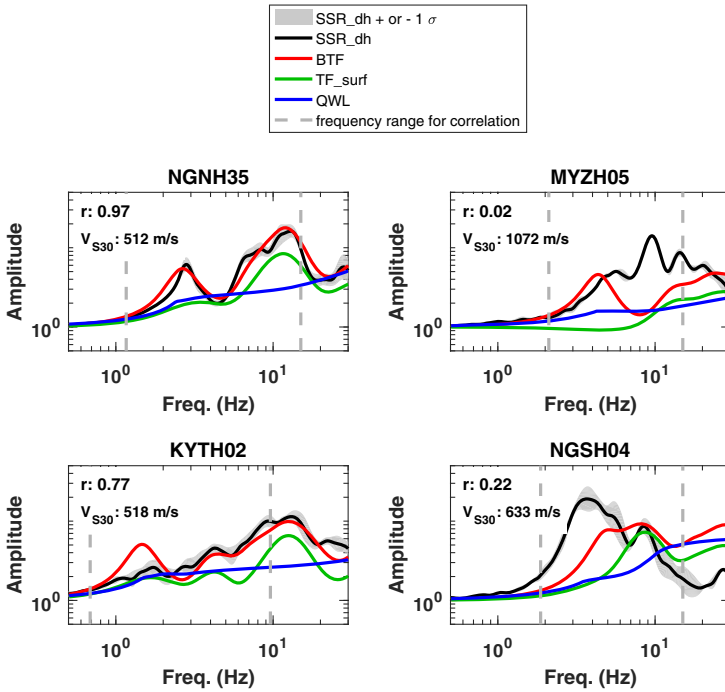


**Fig. 4** Example comparisons between the instrumental site amplification SSR\_dh and the various numerical estimates derived from the velocity profile. The sites selected in the *left column* exhibit a good SSR\_dh/BTF correlation (large r values), while those on the *right* exhibit a bad correlation (low r values). For the 3 numerical methods (BTF, TF\_surf and QWL),  $Q_s$  is defined as  $Q_s = V_s/10$

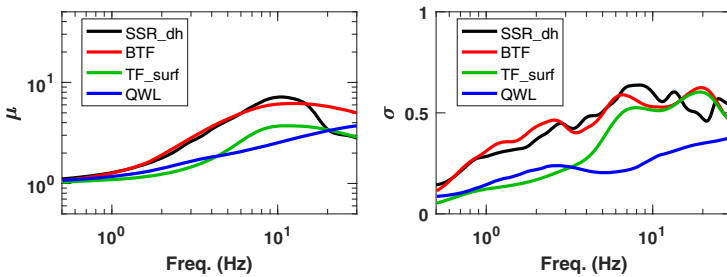


**Fig. 5** Comparison of the mean spectral amplification (*left*) and the mean standard deviation obtained from four different methods for the whole “1D subset” ( $r \geq 0.6$ ). For the 3 theoretical methods (BTF, TF\_surf and QWL),  $Q_s$  is defined as  $Q_s = V_s/10$

sections, the statistical comparison will be limited to these sites. More details on the site selection and distribution of r values may be found in Hollender et al. (2015).

The statistical comparison displayed in Fig. 5 shows that the average site response of this whole “1D subset” is far from being flat but exhibits a significant, broadband amplification around 10 Hz. The mean site responses are relatively similar up to 10 Hz for SSR\_dh and BTF with an amplification around 5–6, while the standard deviation is also similar and large. It is worth mentioning at this stage that the SSR\_dh are in excellent

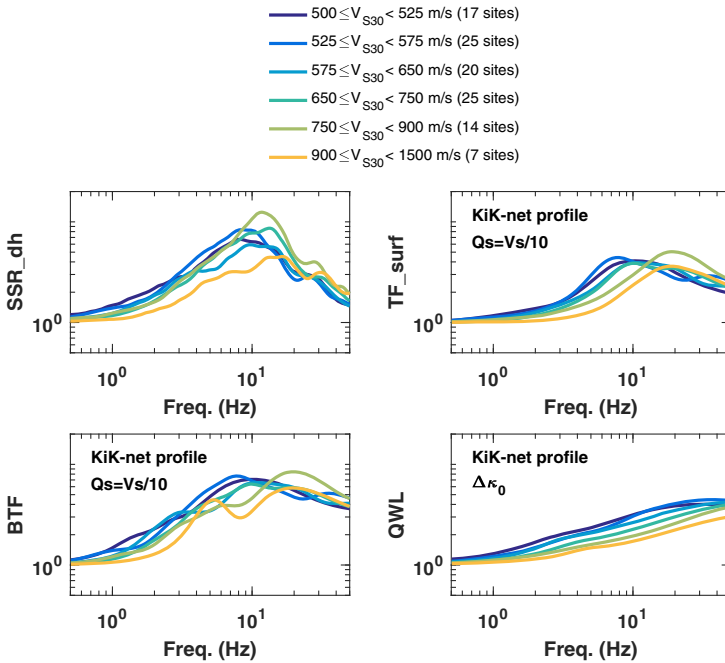


**Fig. 6** Mean empirical (SSR\_dh) and theoretical (BTF) spectral ratios (*left*) and theoretical transfer functions (TF\_surf and QWL) for different  $V_{S30}$  ranges (see Table 2 for the characteristics of each subset)

agreement with the site terms derived from Generalized Inversion Techniques on the same data set (see Hollender et al. 2015). Above 15 Hz, the mean amplification is larger in the case of BTF, which may indicate a bias in the scaling of  $Q_S$ , associated either to an underestimation of the attenuation (too small  $X_Q$ ) or to the non-consideration of a frequency dependence of  $Q_S$  (note however that frequency-dependent  $Q_S$  models include an increase of  $Q_S$  with frequency, while here a decrease would be needed—these models are however derived for deeper crustal propagation, and may not be valid for the shallow depth considered here).

It is also interesting to compare the associated numerical transfer functions TF\_surf with respect to an outcropping reference, with the amplification curves obtained with the QWL method, which is the dominant approach used for the velocity adjustment in the H2T techniques (stochastic modelling based on Boore 2003 approach). As expected, the QWL estimates cannot account for resonance effects (which are expected even in the case of the smooth velocity profiles considered in H2T approaches, see for instance Figure 5 in Boore 2013), and are thus steadily increasing with frequency as a consequence of the average impedance effect at the frequency dependent quarter-wavelength: that is why it does not reproduce the peak around 10 Hz observed in the transfer function. However, without considering the peak, the mean amplitude is relatively similar between TF\_surf and QWL (as discussed by Boore 2013). In addition, the same  $Q_S$  scaling than for BTF is used and again, the amplification level at high frequency is larger than on the observed records. One must keep in mind however that this apparent overestimation occurs in a frequency range (beyond 15–20 Hz), where the instrumental results may be biased by the low-pass filtering

below 30 Hz implemented in the KiK-net pre-processing of KiK-net data, and that interpretation of this high frequency difference should thus be performed with due caution.

Finally, Fig. 6 provides a comparison of the mean empirical and theoretical spectral ratios for different  $V_{S30}$  ranges in order to highlight the evolution of site response with increasing  $V_{S30}$  value. Table 2 presents the characteristics of each  $V_{S30}$  subset, which were selected to have bins having comparable size: it includes the range of  $\Delta\kappa_0$  values obtained from the  $Q_S$  and  $V_S$  profiles (see Eq. 2), which are used for the QWL estimate, together with the  $\kappa_0$  values deduced from the  $\kappa_0$ - $V_{S30}$  relationship of Van Houtte et al. (2011). There are indeed various such relationships in the literature, but this specific one is the most recent one and includes data of previous studies (Silva et al. 1998; Douglas et al. 2010; Drouet et al. 2010; Edwards et al. 2011; Chandler et al. 2006). Besides, this relationship is representative of the main tendency exhibited by all other relationships [see for instance Ktenidou and Abrahamson (2016) or Kottke (2017) for a comparison], except the one of Edwards et al. (2011), which are associated to significantly lower values. Figure 6 indicates that whatever the approach, the mean spectral ratios are shifted towards higher frequency when  $V_{S30}$  increases, as expected since the lower velocity layers are thinner and thinner as  $V_{S30}$  increases. For the 1D estimates BTF and TF\_surf, the evolution with  $V_{S30}$  is more regular than for SSR\_dh, with a slight trend for the peak amplification to be larger for the highest  $V_{S30}$ . For the  $V_{S30}$  range considered here (i.e., 550–1100 m/s), such a behaviour is similar to what is predicted by the QWL estimates used in host-to-target adjustment curves, as they are based on the same velocity and damping profiles. For example, the theoretical adjustment factor (soft-rock-to-rock ratio), showed in the study of Laurendeau et al. (2013) for a soft-rock with a  $V_{S30}$  of 550 m/s and a rock with a  $V_{S30}$  of 1100 m/s and computed in the same way than the one of Van Houtte et al. (2011), presents between 10 and 40 Hz a larger amplification for the rock than for the soft-rock. Around 25 Hz, the theoretical soft-rock-to-rock ratio is around 0.7. On Fig. 6, the ratio between the first TF\_surf curve ( $V_{S30}$  around 525 m/s) and the fifth one ( $V_{S30}$  around 825 m/s) is equal to 0.77. As to the QWL estimates, the low values of  $\Delta\kappa_0$  associated to the  $Q_S$  scaling result in very low attenuation effects, so that the amplification curves hardly exhibit some peak over the considered frequency range (up to 40–50 Hz for the numerical estimates). It must be emphasized that those  $\Delta\kappa_0$  values are found to be significantly smaller than those found in the literature as indicated in Table 2 which provides the  $\Delta\kappa_0$  values estimated from the  $V_{S30}$ - $\kappa_0$  relationship of Van Houtte et al. (2011).

**Table 2** Characteristics of the various subsets with increasing  $V_{S30}$  range used in Fig. 6 and Fig. 14

$V_{S30}$ range (m/s)	Number of sites included	Corresponding range of $V_{Sdh}$ (m/s)	$\Delta\kappa_0$ from $Q_S$ (ms)	Deduced $\kappa_{0\_surf}$ from VH11 (ms)	Deduced $\kappa_{0\_dh}$ from VH11 (ms)	$\Delta\kappa_0$ from VH11 (ms)
500–525	17	1070–2690	1.8–22.6	42.4–44.6	7.5–19.9	23.1–36.5
525–575	25	1100–2780	1.4–5.2	38.5–42.4	7.2–19.3	19.7–34.5
575–650	20	1060–2700	1.2–2.8	33.8–38.5	7.4–20.1	15–28.8
650–750	25	1430–2800	0.9–2.4	29.0–33.8	7.2–14.6	17.8–26.5
750–900	14	1800–3200	0.7–2.1	23.9–29.0	6.2–11.4	16.5–20.4
900–1500	7	1700–2680	0.4–1.1	13.9–23.9	7.5–12.2	6.9–16.3

Only the sites fulfilling the  $r \geq 0.6$  criterion are selected. The used  $\Delta\kappa_0$  values (the differential attenuation term between down-hole and surface) as derived from the known  $V_S$  and assumed  $Q_S$  profiles as indicated in Eq. (2) are listed in column 4, and compared to the expected  $\kappa_{0\_surf}$ - $\kappa_{0\_dh}$  difference derived from the  $V_{S30}$ - $\kappa_0$  empirical relationships of Van Houtte et al. (2011) (columns 5–7)

### 3 Generation of virtual hard rock motion datasets

Considering the successful comparison of SSR\_dh and BTF, it is deemed legitimate to use numerical simulation to deconvolve the surface recordings from the site response in order to obtain estimates of the motion for outcropping hard rock conditions. Two independent approaches are implemented in that aim, and are illustrated on Fig. 7.

- The first type of virtual data is derived from downhole records, through a correction for the depth, or within motion, effects. The corresponding set of hard rock motion is called DHcor.
- The Japanese network offers the opportunity to have for each site two sensors, one at surface and one at depth. However, it is not the case for most other networks, for which only surface data are recorded. This is why a second type of virtual data has been considered, on the sole basis of surface records, corrected for the site response using the known velocity profile; it is called SURFcor. This kind of “site-specific” correction is generally used for a specific site in the target region.
- In addition, the original data, i.e., the actual, uncorrected recordings, are separated in two subsets, DATA\_surf and DATA\_dh (for surface and downhole recordings, respectively), which are used as “control datasets” that allow a comparison with the corrected hard-rock motion estimates.

#### 3.1 Datasets based on corrected downhole records (DHcor)

The downhole records have the advantage to correspond to much larger  $V_S$  values (see Fig. 1 right). However, they are “within” motion affected by frequency dependent interferences between up and down-going waves. Cadet et al. (2012) developed a correction factor to transform them into outcropping motion for surface sites with the same (large)  $V_S$  values. This correction factor modifies the acceleration response spectrum in the dimensionless frequency space  $\nu$  defined by normalizing the frequency by the fundamental destructive interference frequency ( $\nu = f/f_{\text{dest}}$ ). This correction is applied to the KiK-net downhole response spectra, with an underlying assumption of a 1D behaviour. The destructive frequency,  $f_{\text{dest}}$ , is picked directly on the empirical spectral ratios (mainly HVSR\_dh with possible checks on SSR\_dh, see Fig. 3). When this picking of the destructive frequency is unclear on the empirical ratios, it is derived from the theoretical transfer function at depth, TF\_dh. The latter kind of picking of  $f_{\text{dest}}$  had to be done only for

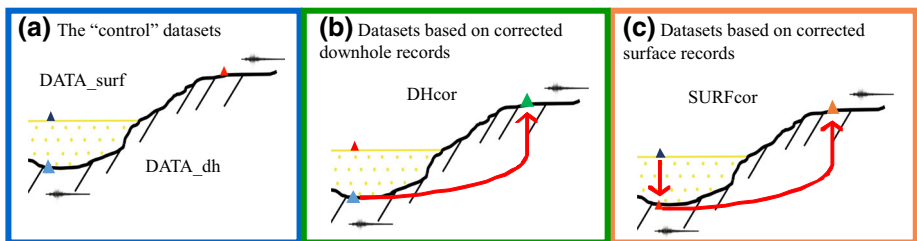


**Fig. 7** Schemes of the different datasets used to develop reference motion GMPEs. The different colors (dark blue, light blue, green and orange) will be used in the following for the results corresponding to each of those datasets

14 sites, while the former could be achieved directly on empirical ratios for 138 recording sites.

A total of 1031 records could finally be used to build this first dataset DHcor of corrected downhole motion and to develop an associated GMPE (see Table 1). For the original, uncorrected datasets (DATA\_dh and DATA\_surf), the same collection of events and sites is used.

### 3.2 Datasets based on corrected surface records (SURFcor)

Considering that the KiK-net network is the only large network involving pairs of surface and downhole accelerometers at each site, we tested here another way to derive hard rock motion directly from the surface records (SURFcor), by using the velocity profiles down to the downhole sensor to deconvolve the surface motion from the linear site transfer functions with a SH-1D simulation code.

The correction approach (designated as SURFcor) consists in estimating the outcropping hard rock motion, on the basis of Fourier domain deconvolution. The Fourier transform of each surface signal is computed and then divided by the SH-1D transfer function with respect to an outcropping rock consisting of a homogeneous half-space with a S-wave velocity equal to the velocity at the depth of the down-hole sensor. This estimated outcropping rock spectrum is then converted in time domain by inverse Fourier transform, and the associated acceleration response spectrum is computed.

To apply such a deconvolution correction, only sites with a probable 1D behaviour (i.e., with a correlation coefficient between the empirical and the theoretical ratios larger than 0.6 are selected, as proposed by Thompson et al. (2012). Once again, only the records associated to a site and an event having recorded at least three records are selected. This leads to a set of 765 records (see Table 1).

Some variants of this approach were also tested as a sensitivity analysis, in order to check the robustness of the results (see Laurendeau et al., 2016). Several  $Q_S$ —velocity scaling were considered, corresponding to  $X_Q$  values in Eq. (3) ranging from 5 (low damping) to 50 (large damping), and several incidence angles were also considered, from  $0^\circ$  to  $45^\circ$ . An alternative approach often considered in engineering is to perform the “deconvolution” directly in the response spectrum domain: it was also tested here through an average “amplification factor” derived from the same 1D simulations for a representative set of input accelerograms; it is not, however, the recommended procedure as the response spectrum amplification factor differs for the Fourier transfer function in that it depends not only on the site characteristics but also on the frequency contents of the reference motion.

### 3.3 Direct comparison of the response spectra from the different methods

The different corrections applied to the observed data are based on several assumptions which allow corrections on a large database. These corrections are not intended to be fully valid in the case of one particular record, but mainly in a statistical way. However, it is still interesting to analyse the effect of the corrections for a given record, to highlight their advantages and disadvantages: Fig. 8 presents a few examples for the three sites already considered in Fig. 3.

To test the DHcor method, MYGH06 is a relevant site because it is characterized by a flat SSR\_dh (Fig. 3), except at the destructive frequency. A good agreement is observed between DHcor and DATA\_surf (Fig. 8a), providing an indirect check of the depth effect



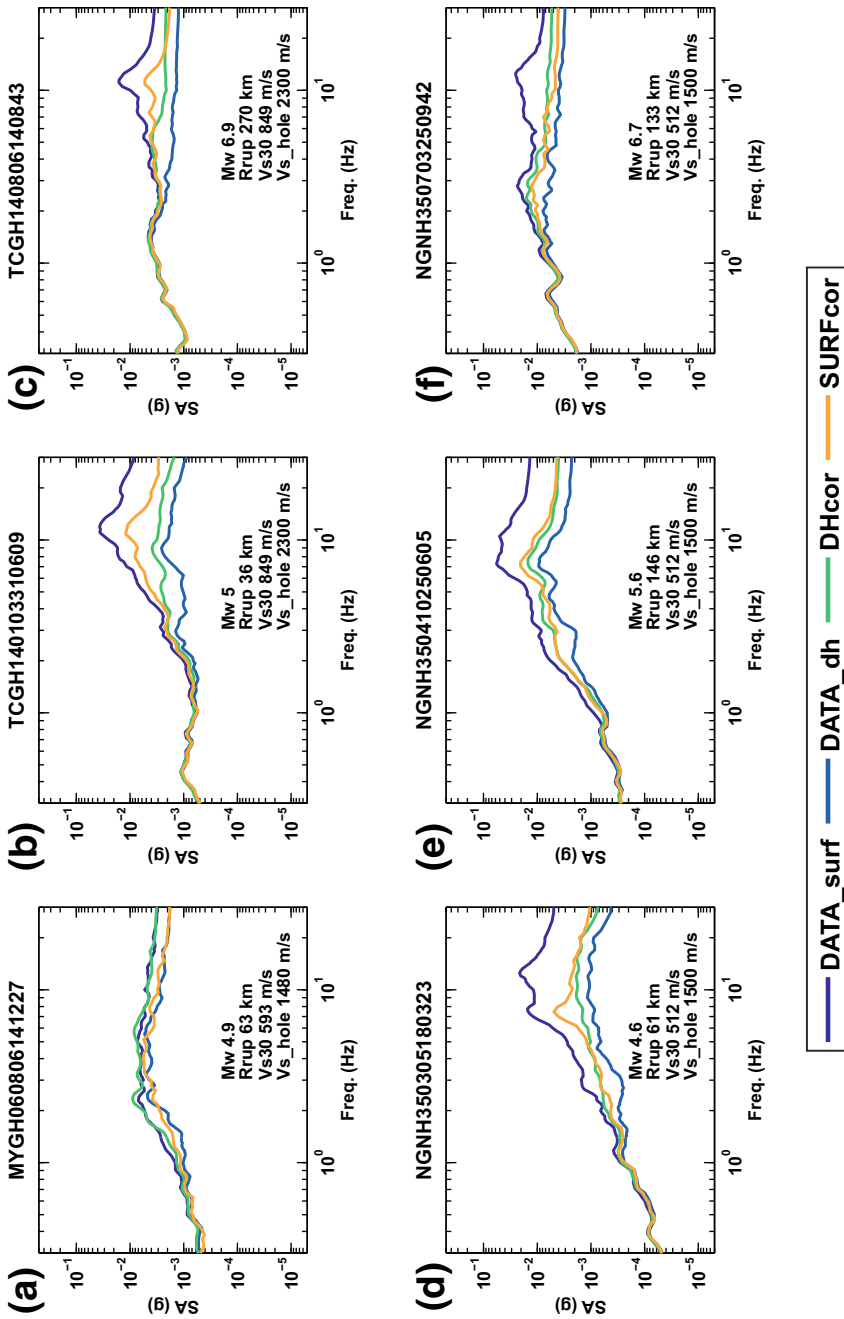


Fig. 8 Comparison of the response spectra for different events recorded at three different stations obtained from the four datasets

correction factor of Cadet et al. (2012). On the contrary, SURFcor displays slightly lower amplitudes, probably due to a larger correction factor linked with the shear wave velocity contrast at shallow depth. In fact, at high frequency the theoretical amplification looks as insufficiently attenuated for this example. The same behaviour is observed at the same site for different magnitude-distance scenarios.

The comparison has been also performed for two other example sites characterized by a SSR\_dh with large amplification at high frequency (see Fig. 3). For TCGH14 (Fig. 8b, c), the site amplification seems insufficiently corrected around the peak for all the scenarios tested (two are shown here), as SURFcor is larger than DHcor. For NGNH35 (Fig. 8d–f), the response spectra are relatively similar for the intermediate scenarios. The largest differences are observed for the extreme scenarios. The response spectrum of SURFcor appears insufficiently corrected for the smaller magnitude event, while it appears slightly over corrected at high frequency for the larger magnitude event. Indeed, it has been shown repeatedly that the actual site response presents a significant event-to-event variability (which could be related to incidence or azimuthal angles, as shown in Maufroy et al. 2017), and the observed variability of the event-to-event differences between SURFcor and DHcor estimates is certainly linked to such variability, as both SURFcor and the DHcor corrections are based on average response. However, as will be shown in the next “GMPE” section, the two corrections lead to very similar median predictions, with a larger variability for the SURFcor approach, which is consistent with the few examples shown here. One may notice also on these few examples that the corrected spectra are always in-between the uncorrected surface and down-hole spectra: hard-rock outcropping motion is found to be (significantly) lower than the stiff or standard-rock motion. The next section is devoted to investigate to which extent such a result can be generalized and quantified.

#### 4 Comparison in terms of GMPE results

To analyse the overall behaviour of those different real or corrected datasets, we have chosen to develop ground motion prediction equations based on a simple functional form in order to get the coefficients directly. Indeed, the functional forms used in the literature are increasingly complex, requiring fixing some coefficients, which is preformed beforehand on the basis either of a theoretical simulation or of an empirical analysis of a well-controlled subset. Given the distribution of our dataset (see Fig. 1), with almost no data in the near field of large events, and given our focus on the site term, we consider such a simple functional form to be appropriate for our goal. The “random effects” regression algorithm of Abrahamson and Youngs (1992) is used to derive GMPEs for the geometrical mean of the two horizontal components of SA (expressed in g). The following simple functional form is used:

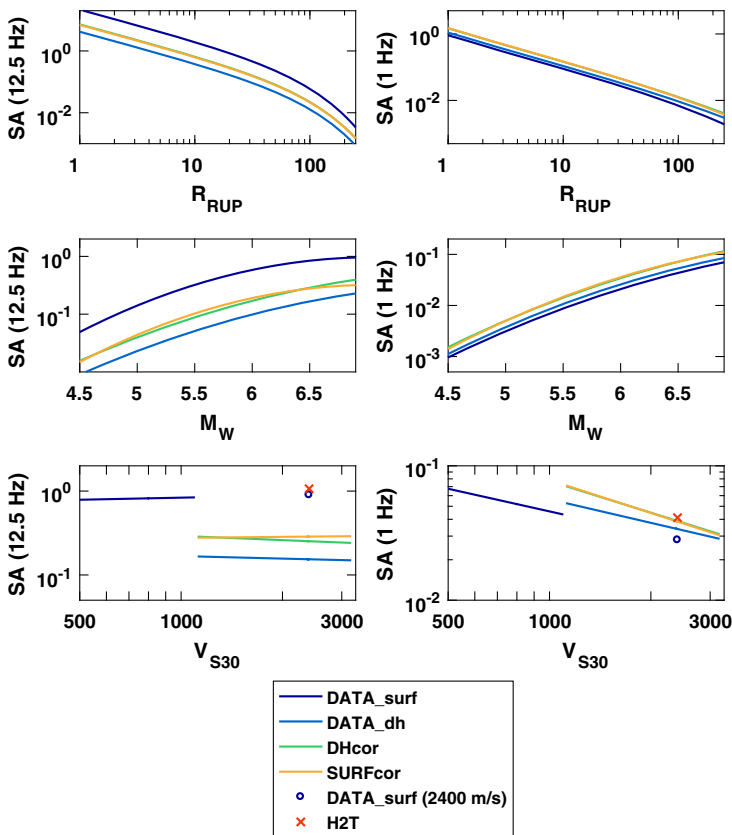
$$\ln(\text{SA}(\text{T}))_{\text{es}} = a_1(\text{T}) + a_2(\text{T}) \cdot M_{\text{W}} + a_3(\text{T}) \cdot M_{\text{W}}^2 + b_1(\text{T}) \cdot R_{\text{RUP}} - \ln(R_{\text{RUP}}) + c_1(\text{T}) \cdot \ln(V_{\text{S}}/1000) + \delta B_{\text{e}}(\text{T}) + \delta W_{\text{es}}(\text{T}) \quad (5)$$

where  $\delta B_{\text{e}}$  is the between-event and  $\delta W_{\text{es}}$  the within-event variability, associated with standard deviations  $\tau$  and  $\varphi$  respectively, and  $\sigma_{\text{TOT}} = (\tau^2 + \varphi^2)^{0.5}$ .  $V_{\text{S}}$  is either  $V_{\text{S30}}$  (for the control set DATA\_surf) or the velocity at down-hole sensor  $V_{\text{SDH}}$  (for the three other datasets, real or virtual), which is assumed to be very close of the average velocity over the 30 meters immediate below the down-hole sensor, especially when compared to the high

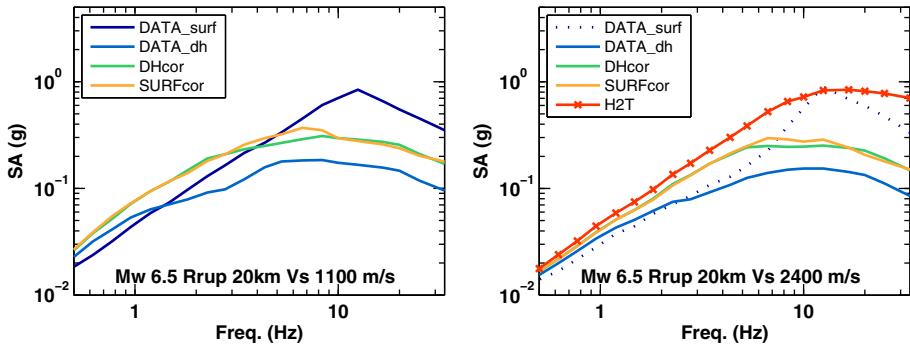
values at depth. That is why, in the following,  $V_{S30}$  is also used for  $V_S$  values for very hard rock sites. The resulting coefficients are given in the supplement electronic.

Figure 9 shows the predicted spectral acceleration with all the models (DATA\_surf, DATA\_dh, DHcor, SURFcor) as a function of the distance, the magnitude, and  $V_{S30}$  for two frequencies ( $f = 12.5$  Hz and  $f = 1$  Hz). Figure 10 displays a comparison of the motion predicted for a given earthquake scenario ( $M_W = 6.5$ ,  $R_{RUP} = 20$  km) and two  $V_S$  values (1100 and 2400 m/s). The first one corresponds to a  $V_{S30}$  value which is common to each dataset. The second one was chosen so as to make a comparison with a H2T method, and especially with the  $V_S$  of the Van Houtte et al. (2011) adjustment factor. These comparisons call for several comments.

First, the DHcor and SURFcor models give very similar predictions in term of median. The main differences with the “control datasets” (DATA\_surf and DATA\_dh) are observed at high frequency. DATA\_surf presents the largest values at high frequency, while the lowest amplitudes are associated to DATA\_dh: the latter is the only model that corresponds to within motion on hard rock, always smaller than outcropping motion for similar velocity. DATA\_surf is larger because most of the sites are presenting significant to large amplification peaks at high frequency linked to shallow, lower velocity layers. These



**Fig. 9** Predicted spectral acceleration (SA) at 12.5 Hz (top) and 1 Hz (bottom) as a function of  $R_{RUP}$  (with  $M_W = 6.5$  and  $V_{S30} = 1100$  m/s, left),  $M_W$  (with  $R_{RUP} = 20$  km and  $V_{S30} = 1100$  m/s, middle) and  $V_{S30}$  (with  $M_W = 6.5$  and  $R_{RUP} = 20$  km, right)



**Fig. 10** Comparison of the predicted SA obtained with the empirical models for two  $V_S$  values and for a specific scenario  $M_W = 6.5$  and  $R_{RUP} = 20$  km. The models are presented with *dashed lines* when the  $V_S$  value is outside the range of  $V_S$  used to develop the model

site effects obviously do not affect DHcor predictions, and are “statistically” removed with the SURFcor approach.

Between DHcor and SURFcor, small differences are observable mainly at the limits of the model, i.e., large distances or large magnitudes. The main (though still slight) differences correspond to the  $V_{S30}$  dependency at high frequency (see Fig. 9). At low frequency, as expected, the spectral acceleration decreases with increasing  $V_S$  (the site coefficient  $c_1$  is negative). However, at high frequency, when  $V_S$  increases, the spectral acceleration stays almost stable for SURFcor and DATA\_surf (the site coefficient  $c_1$  is close to zero). This unexpected observation will be commented later in the Sect. 5, but one may notice that the same behaviour is observed for the DATA\_surf GMPE: this maybe corresponds to the fact that when the range of  $V_{S30}$  is too small and the actual dependency only weak, there might be a trade-off between the  $V_{S30}$  dependency ( $c_1$  term) and the constant term ( $a_1$  term), leading to the jumps in the  $c_1$  coefficient between DATA\_surf and the other sets. This led us to derive other GMPEs by mixing the DATA\_surf set with the hard rock sets, in order to cover a much wider range of  $V_{S30}$  values, as will be discussed later.

Figure 10b also includes an example comparison with typical H2T predictions for a  $V_S$  of 2400 m/s, according to the correction factors proposed in Van Houtte et al. (2011). As indicated in the introduction, this specific H2T implementation has been used here because it was taking into account the widest set of  $V_{S30}$  and  $\kappa_0$  measurements available by the time we started the present study. The H2T amplitude based on the accepted  $V_{S30}$ – $\kappa_0$  relationship, is found to be 3–4 times larger at high frequency ( $f > 10$  Hz) compared to DHcor and SURFcor. The H2T amplitude is obtained after the adjustment of DATA\_surf predictions for a  $V_{S30}$  of 800 m/s, which have also larger amplitude at high frequency than the other models.

Figure 11 shows the variation of variability with frequency associated with the predicted spectral accelerations. The total variability ( $\sigma_{TOT}$ ) associated with the different datasets is mainly controlled by the within-event variability ( $\phi$ ) because the between-event variability ( $\tau$ ) is relatively stable between models. The within-event variability is lower for the models based on downhole records: DHcor and DATA\_dh, indicating that the site to site variability is significantly lower at depth for a given velocity range. The within-event variability is larger for the entire range of frequency in the case of DATA\_surf. The within-event variability is larger also around 10 Hz for SURFcor, which corresponds to the average amplification peak observed for the stiff-soil/soft rock sites considered here.

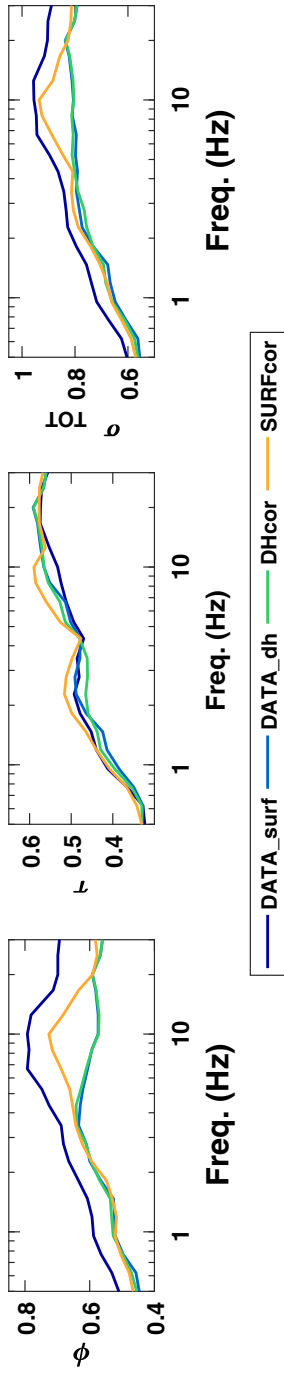


**Fig. 11** Within-event (*left*), between-event (*middle*) and total (*right*) aleatory variability

## 5 Discussion

These hard-rock motion prediction results provide the basis for two main types of comparisons and discussions, which are presented sequentially in this section: first the inter-comparison of the two independent correction approaches from down-hole and surface recordings, and second, as they are very consistent with each other, their comparison with the hard-rock estimates using the Campbell (2003) H2T approach with Van Houtte et al. (2011)  $V_{S30}-\kappa_0$  relationship.

### 5.1 Comparison of DHcor and SURFcor predictions

The GMPE comparison highlights a very good agreement between the average predicted spectral acceleration of DHcor and SURFcor in the case of the tested scenarios (Figs. 9, 10). Although very slight differences may be observed as to their  $V_{S30}$  dependence at high frequency (see Fig. 9), the main difference between SURFcor and DHcor models lies in the amount of within-event variability, which is larger for SURFcor at high frequency (see Fig. 11). Around 10 Hz (the average amplification peak of the stiff sites constituting the dataset, see Fig. 5), this variability is close to the one of DATA\_surf for SURFcor. The variability associated to SURFcor could be explained by a non-adequate correction of site effect, linked with inadequate velocity or damping profiles (even though there has been a tough selection of “1D” sites in the present study).

Firstly, this larger variability on SURFcor could be explained at least partly by the inadequateness of the 1D correction, even though only the sites with an a priori 1D behaviour and/or with good parameters to explain the observations [for example, appropriate definition of  $V_S(z)$ ] were selected to implement the SURFcor dataset. The selection criterion as we applied it ( $r \geq 0.6$ ) allows to keep a reasonably large number of sites and recordings (two-thirds, see above). However, in view of applying this correction to other networks with only surface recordings, empirical spectral ratios are not always available to constrain the validity of the 1D assumption. That is why a sensitivity test was performed, with different threshold levels for the  $r$  value: without any threshold (i.e., all sites, 1004 records, 79 events and 138 sites),  $r \geq 0.6$  (704 records, 70 events and 97 sites),  $r \geq 0.7$  (564 records, 63 events and 76 sites) and  $r \geq 0.8$  (334 records, 41 events and 45 sites). The results are displayed on Fig. 12 left for the median estimates for a specific scenario, and on the right for the corresponding aleatory variabilities. The median estimates are found to exhibit only a weak sensitivity on the “1D selection”, especially when compared with the difference with H2T estimates. A larger sensitivity is found on the within-event variability, especially in the high-frequency range (beyond 3.5 and 5 Hz): it is the largest in the case without any 1D selection and decreases when the selection is more restrictive (higher correlation coefficient). For the most stringent one ( $r \geq 0.8$ ), the within-event variability is closer to the one found for DHcor. This suggests that the physical relevancy of the procedure used for the correction of surface records for local site effects is an important element in reducing the variability associated with hard rock motions. One must however remain cautious in commenting such results, since the number of available data drops drastically when the 1D acceptability criterion becomes too stringent.

Secondly, this larger variability on SURFcor could also be partly explained by the selected  $Q_S$  values used to compute the theoretical site transfer function. In this study, we have used the standard scaling  $Q_S = V_S/10$  as it is widely used in earthquake engineering applications (e.g., Fukushima et al. 1995; Olsen et al. 2003; Cadet et al. 2012; Maufroy

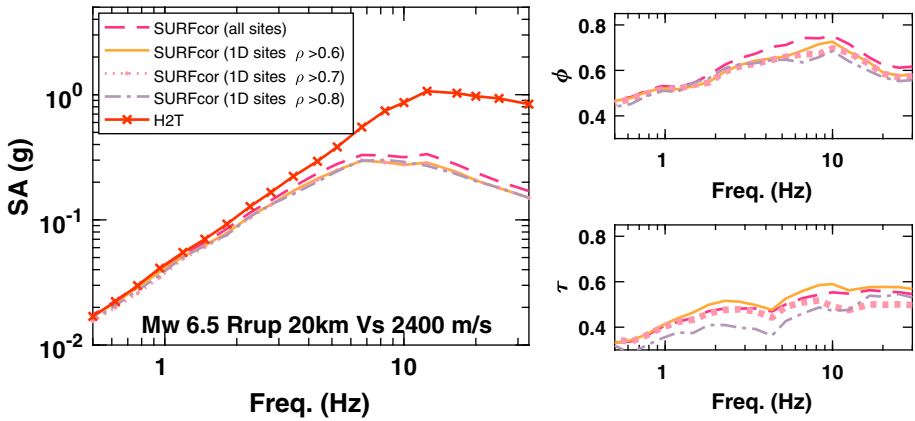


**Fig. 12** Effect of the “1D” selection of sites on predicted SA for SURFcor (*left*) for a specific scenario ( $M_W = 6.5$ ,  $R_{RUP} = 20$  km) on a hard-rock site ( $V_S = 2400$  m/s), and on the within-event  $\phi$  (*right top*) and between-event  $\tau$  (*right bottom*) variability

et al. 2015). However, even if this model allows a satisfactory average fit to the observed site amplification up to 10 Hz (Fig. 5), it is not the best for all sites and especially, in the high frequency range. We have thus investigated the sensitivity of the SURFcor correction to  $Q_S$  by deriving alternative “SURFcor” virtual datasets with different  $Q_S$ – $V_S$  scaling. The results are illustrated in Fig. 13 for the extreme case of very high damping ( $X_Q = 50$ , i.e.,  $Q_S = V_S/50$ ). It turns out that the median estimates (shown here for the same scenario) are not significantly affected by the damping scaling, even at high frequency, while the within-event variability is found significantly larger at high frequency ( $f > 4$ –5 Hz) for the larger damping values. An optimal option might be to define for each site the “best  $Q_S$  profile” in a similar way to what was done by Assimaki et al. (2008), with however the risk of a significant trade-off between shallow velocity profiles and  $Q_S$  values at

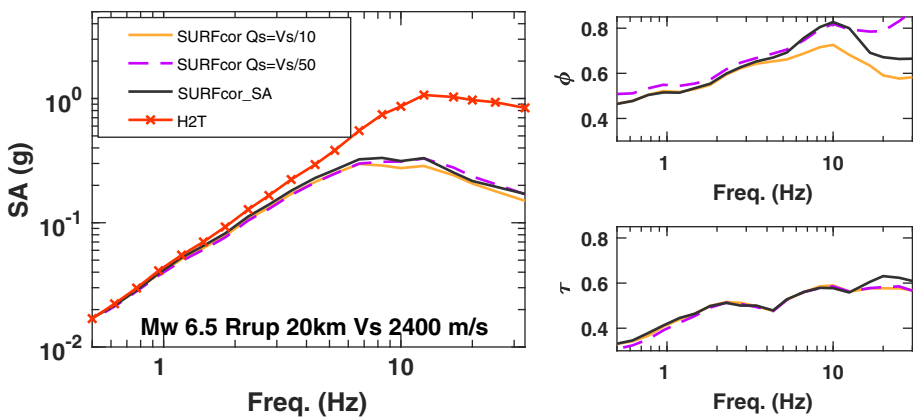


**Fig. 13** Sensitivity tests on the SURFcor approach: effects on the median predictions (*left*) and on the aleatory variability (within-event  $\phi$ , *top right*; between-event  $\tau$ , *bottom right*) of the  $Q_S$ – $V_S$  scaling and of the deconvolution approach (Fourier spectra or response spectra: SA). The considered scenario is the same as in previous figures:  $M_W = 6.5$ ,  $R_{RUP} = 20$  km, hard-rock with  $V_S = 2400$  m/s). Also shown is the H2T prediction for the same scenario

high frequency. Also, it could be possible to consider a frequency-dependent  $Q_s$  [ $Q_s(f) = Q_{s0} \times f^\alpha$ ]. Recent investigations on the internal soil damping descriptions between surface and depth for a few KiK-net sites corresponding EC8 B/C class (E. Faccioli, personal communication), suggest that  $Q$  is linearly increasing with frequency ( $\alpha = 1$ ). In our case however, the average results displayed in Fig. 5 for the numerous EC8 A/B sites considered here indicate an overestimation of the mean spectral amplification for higher frequencies with  $Q_s = V_s/10$ . It appears necessary to reduce  $Q_s$  (or to increase  $X_Q$ ) at high frequency to fit the observations. Such findings might be an indirect indication that the scaling parameter  $X_Q$  should be depth dependent with larger values at shallower depth/ or for softer material, which could then be combined with a frequency dependence. In any case, this also indicates that there is definitely a need for further research on the soil damping issue, starting with reliable measurement techniques.

Finally and incidentally, we deem it worth mentioning a few words about the “deconvolution approach” when it is performed in the response spectrum domain through the use of amplification factors, as often done in the engineering community in relation to site response, for instance in all GMPEs. It was performed here simply as a sensitivity test to investigate the potential differences between a correction in Fourier (FSA) and response spectra (SA) domains. As amplification factors on response spectra are known to be sensitive to the frequency contents of the input motion, this SA correction was implemented here through an average amplification factor derived for each site from its response to 15 accelerograms selected in the RESORCE European databank (Akkar et al. 2014) to cover a wide range of frequency content, with spectral peak varying between 1 and 20 Hz. More details can be found in Laurendeau et al. (2016). Figure 13 shows that SURFcor\_FSA and SURFcor\_SA result in similar predictions in terms of median response spectra, with however a much larger high-frequency within-event variability for SURFcor\_SA. This larger variability is interpreted as due to the highly nonlinear scaling of response spectra with respect to Fourier spectra computation, especially in the high-frequency range (Bora et al. 2016): the larger variability at high frequency is due to the use of average amplification factors on response spectra instead of record specific amplification factors.

## 5.2 Comparison with the classical H2T approach using the Van Houtte et al. (2011) $V_{S30}-\kappa_0$ relationship

Despite these issues on high frequency variability, the main outcome of this study is to point out an important difference in the median amplitude of the high frequency motion predicted by the Van Houtte et al. (2011) H2T approach on the one hand (which has been repeatedly shown to provide adjustment factors comparable to those obtained with other H2T methods, see Ktenidou and Abrahamson 2016), and by the different “hard-rock” GMPEs derived here (DHcor and SURFcor) on the other hand. The H2T corrections applied here are based on the GMPE predictions obtained from surface records (DATA\_surf) for  $V_{S30} = 800$  m/s, adjusted to a hard rock characterized by a  $V_s$  around 2400 m/s with the Van Houtte et al. (2011) adjustment factor. The latter is tuned to the  $\kappa_0$  values provided by the  $V_{S30}-\kappa_0$  relationships derived by the same authors from worldwide data. This model is compared with the predictions from other datasets only for  $V_{S30} = 2400$  m/s (see Figs. 9, 10). For hard rock with velocities beyond 2 km/s, the H2T estimate is found to be 3–4 times larger at high frequency ( $f > 10$  Hz) compared to DHcor and SURFcor, while it decreases with decreasing frequencies, to become negligible at low frequency ( $f < 1$  Hz): in the low frequency domain, the key parameter is the velocity, and



it is worth noticing the QWL impedance approach provides correction factors very similar to those obtained by 1D deconvolution. As shown in Figs. 11 and 12, the high-frequency difference is a robust result, as it remains large and similar for all the performed sensitivity tests: correction procedure (from down-hole or surface recordings, in the Fourier or response spectra domains), 1D site selection, and  $Q_S-V_S$  scaling). The origin of so large differences should be looked for in the specificities and assumptions in either approach: H2T on the one hand, and correction procedures for virtual data sets DHcor and SURFcor on the other hand. Both are explored and discussed in the next paragraphs.

A first origin may be associated, in different ways, to the amount of high-frequency amplification on stiff to standard-rock sites and the way it is accounted for. The adjustment factor technique (H2T), is applied to DATA\_surf GMPE, which is based on recordings which were shown earlier in this work to have a much larger high-frequency amplitude than DATA\_dh, in relation with the shallow velocity profile. The H2T adjustment procedure should therefore, in principle, account for such a high-frequency amplification. However, as shown in Figs. 4, 5 and 6, it is not properly reproduced by the QWL method, which only accounts for average impedance effects between deep bedrock and shallow (frequency-dependent) depth, while the surface to down-hole transfer functions (both instrumental and theoretical) suggest significant resonance effects due to shallow velocity contrasts. Besides, the velocity correction used for the adjustment factor of Van Houtte et al. (2011) and almost all H2T approaches (Campbell 2003 as well as Al Atik et al. 2014) is computed from generic velocity profiles (Boore and Joyner 1997; Cotton et al. 2006), which are probably not optimally suited to the KiK-net database. Indeed, Poggi et al. (2013) defined a reference velocity profile ( $V_{S30}$  of 1350 m/s) from the KiK-net database which present a stronger impedance contrast in the first 100 m, consistently with findings of an earlier work by Cadet et al. (2010). Figure 14 presents QWL amplification curves computed with the generic velocity profiles (Boore and Joyner 1997; Cotton et al. 2006) tuned to the  $V_{S30}$  value and truncated at the depth of the down-hole sensor; the site classes (i.e.,  $V_{S30}$  ranges) are the same as in Fig. 6, and the damping effect are the same, i.e., with  $\Delta\kappa_0$  deduced from  $Q_S(z)$ . In comparison to results in Fig. 6, it is clear that the QWL correction is sensitive to the velocity profile: the Boore and Joyner (1997) generic profiles

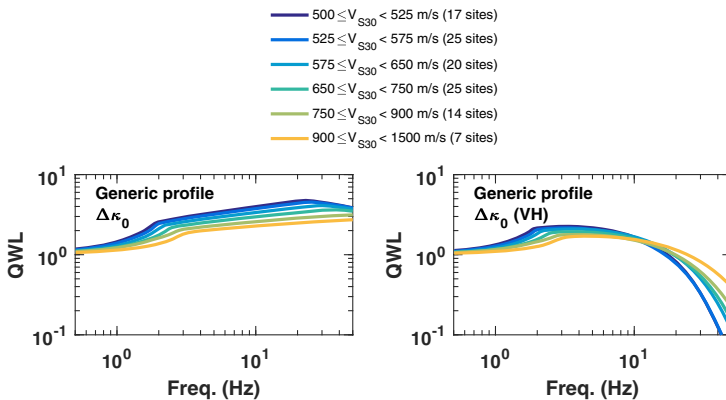


**Fig. 14** Theoretical QWL amplification functions computed from the generic profile for different  $V_{S30}$  ranges, with a maximal depth corresponding to down-hole sensor depth, and with two different values of  $\Delta\kappa_0$ : on the *left* it is derived from the  $V_S$  and  $Q_S$  profiles as in Fig. 6, while on the *right* it is estimated from the empirical relationships of Van Houtte et al. (2011) (see Table 2 for the characteristics of each subset)

predict slightly larger and broader frequency amplification (i.e., starting at lower frequency) than the actual KiK-net profiles with their larger velocity gradient at shallow depth. However, the noticeable difference does not fully explain the large high-frequency difference between H2T and our approaches, which is also probably related to  $\kappa_0$  values, as discussed in the next section.

Another reason for these high-frequency differences may be related to the site characterization scheme: in the H2T approach, it is based on the twin proxy ( $V_{S30}$ ,  $\kappa_0$ ), which is however often reduced to  $V_{S30}$  only through  $V_{S30}$ - $\kappa_0$  relationships as those proposed by Van Houtte et al. (2011) when no site-specific measurement of  $\kappa_0$  is available. For the DHcor set, it is based on the down-hole velocity  $V_{SDH}$  and the measured destructive interference frequency  $f_{dest}$  (related to the travel time between the surface and downhole sensors, i.e., on the surface-downhole average velocity). For the SURFcor sets, it is based on the full S-wave velocity profile (and the related assumptions on unit mass and damping profiles). The two latter thus involve more to much more details about the velocity profile, used before the derivation of GMPEs, while the former (H2T) combines a velocity proxy and a damping proxy (sometimes simply inferred from the velocity proxy or IRVT), which are used as a post-correction of GMPE results for “standard rock” sites, on the basis of stochastic modeling. It is thus not so easy to compare the results obtained in a very different way. Two items may however be discussed: the site term in the GMPEs, and the  $\kappa_0$  values and their relationship with  $V_{S30}$ .

- The site term in SURFcor and DHcor GMPEs is characterized by the coefficient  $c_1$  controlling the  $V_{S30}$  dependence. It could indeed implicitly account, at least partially, for a “hidden correlation” between  $\kappa_0$  and  $V_{S30}$ . As shown in Fig. 9,  $c_1$  is found close to zero at high frequency, which may reflect some slight decrease of  $\kappa_0$  with increasing  $V_{S30}$ .
- This  $V_{S30}$  dependence must however be investigated further, as Fig. 9 indicates a “step-like” difference between DATA\_surf ( $500 \leq V_S \leq 1000$  m/s) and the other models ( $1000 \leq V_S \leq 3000$  m/s) for sites having velocities close to their intersection zone, i.e., around 1000 m/s. For instance, the predicted amplitude is significantly higher at high frequency (0.84 g for DATA\_surf for SA (12.5 Hz) instead of around 0.3 g for the others), and slightly lower at low frequency (0.04 g compared to 0.07 g for the others). To eliminate the  $V_S$  gap between the two datasets, a new set of GMPEs has been derived by mixing the DATA\_surf set and the corrected outcropping hard-rock virtual datasets (DHcor or SURFcor), which allows to explore a much larger  $V_S$  range ( $500 \leq V_S \leq 3000$  m/s). The corresponding results displayed in Fig. 15 replace the “jump” by a continuous, decreasing dependence on  $V_S$ , at all frequencies. To further investigate whether this “smoothing” of the jump is real or imposed by the “ $c_1 \cdot \log(V_S)$ ” functional form, Fig. 16 displays the dependence of within-event residuals with  $V_S$  for the “DATAsurf + SURFcor” case, without (left) and with the “ $c_1 \cdot \log(V_S)$ ” site term (right). The left plot actually supports the existence of the jumps identified in Figs. 9 and 15, especially at high frequency, while the right plot indicates the classical functional form performs rather well in reducing the residuals. This suggests that, even though the correction procedures of downhole or surface recordings can probably be improved to remove these jumps, there is a definite trend for hard rock motion to be significantly lower than standard rock motion, even at high frequency.

$\kappa_0$  effects also deserve specific discussion, mainly because the high-frequency increase of ground motion predicted for very hard-rock sites by the H2T approach is essentially controlled by  $\kappa_0$  values, which are generally assumed to be very low on hard rock sites (see

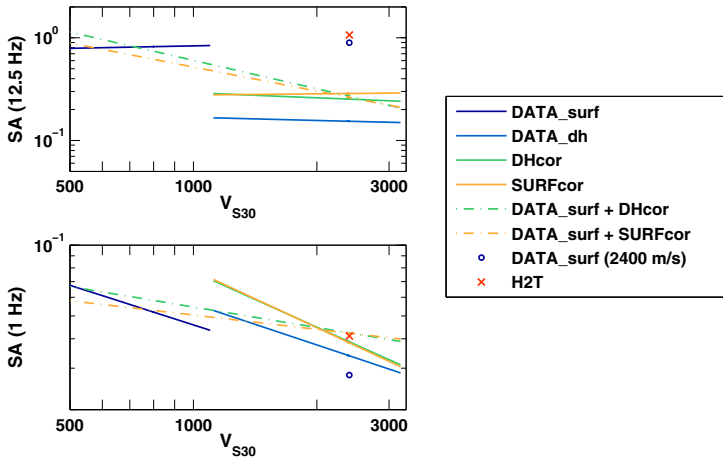


**Fig. 15** Comparison of the predicted spectral acceleration (SA) at 12.5 Hz (*left*) and 1 Hz (*right*) as a function of  $V_{S30}$  for GMPEs derived from data with varying  $V_S$  ranges. *Solid lines* correspond to “homogeneous” datasets (DATA\_surf; DHcor, SURFcor, DATA\_dh), while *dotted lines* correspond to “hybrid” datasets (DATA\_surf + DHcor, DATA\_surf + SURFcor)

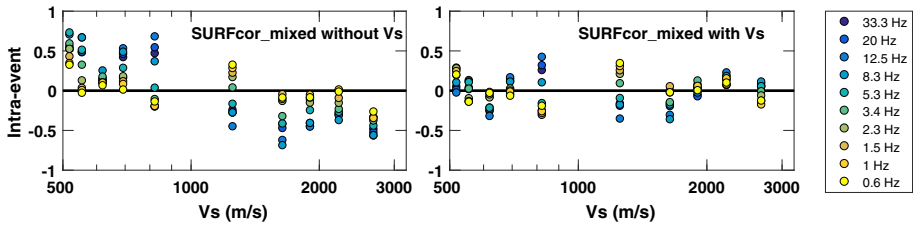


**Fig. 16** Dependence of the mean within-event residuals as a function of  $V_S$  for different frequencies (*color code on the right*) for the GMPEs derived from hybrid set DATA\_surf + SURFcor. *Left* no site term is considered in the functional form of the GMPE; *right* with a “ $c_1 \cdot \log(V_S)$ ” site term. The mean within-event residuals are computed for bins of 150 data points and represented for the corresponding geometrical mean of  $V_S$  values

Van Houtte et al. 2011 and the recent reviews on  $V_{S30}-\kappa_0$  relationships: Kottke 2017; Biro and Renault 2012).

- It should first be noticed that, as shown by Parolai and Bindi (2004), the significant amount of high-frequency amplification (linked with shallow layers) observed at “standard rock” surface, may bias the  $\kappa_0$  measurements, leading to overestimations when the spectral fall-off frequency range is located beyond the site fundamental frequency (“standard rock”) and conversely to underestimations when the site fundamental frequency is beyond the measurement range (which is more likely to happen for hard rock sites).
- For all the KiK-net sites considered here, it is found that (a) the impact of the damping in the layers between the down-hole and surface sensors is not enough to kill the high-frequency amplification—at least for commonly accepted  $Q_S-V_S$  scaling, see Fig. 13—and that (b) the associated  $\Delta\kappa_0$  changes (i.e., the down-hole to surface increase in  $\kappa_0$ ) is much lower than the one predicted by Van Houtte et al. (2011) or the other similar

$V_{S30}-\kappa_0$  relationships. Even though the values listed in Table 2 correspond to the median  $Q_S$  scaling,  $Q_S = V_S/10$ , the ratio between VH2011 and SURFcor  $\Delta\kappa_0$  values is around a factor of 10 for every  $V_{S30}$  range. The impact of such a huge difference is displayed in Fig. 14 which compares the QWL estimates of amplification curves with both sets of  $\Delta\kappa_0$  values. In other words, a  $Q_S$  scaling around  $Q_S = V_S/100$  (i.e., a  $Q_S$  of 10 for a S-wave velocity of 1000 m/s) would be needed to explain the increase of high-frequency motion on very hard rock site. Such a scaling seems a priori unlikely.

- Another possibility is that  $\kappa_0$  actually corresponds to the effect of damping over a much larger depth than the one involved in KiK-net sites (mostly 100 and 200 m). This would however be somewhat inconsistent with the fact that most of the amplification pattern is well reproduced by the velocity structure over this limited depth, as shown by Hollender et al. (2015).

Further investigations on the actual values, meaning and impact of  $\kappa_0$  are thus definitely needed, through careful measurements after deconvolution from the high-frequency amplification effects.

Figure 17 finally summarizes an important outcome of the present study, with the ratios or predicted ground motion between standard rock ( $V_{SH} = 800$  m/s) and hard-rock ( $V_{ST} = 2400$  m/s) sites, compared with the ratios derived from the classical H2T method (Campbell 2003) and the  $V_{S30}-\kappa_0$  relationship compiled by Van Houtte et al. (2011). When the  $V_S$  range lies within the validity range of a given GMPE, such a ratio may be derived simply from the site term (i.e., the value of  $c_1 \cdot \log(V_{ST}/V_{SH})$ ): this is possible only for the 2 hybrid GMPEs (DATA\_surf + SURFcor) and (DATA\_surf + DHcor). The ratio was also computed for a given scenario event ( $M_W = 6.5$ ,  $R_{RUP} = 20$  km) from the response spectra estimated with different GMPEs (i.e., DATA\_surf for standard rock, and SURFcor or DHcor for hard rock). As can be expected from the previous comparisons and sensitivity

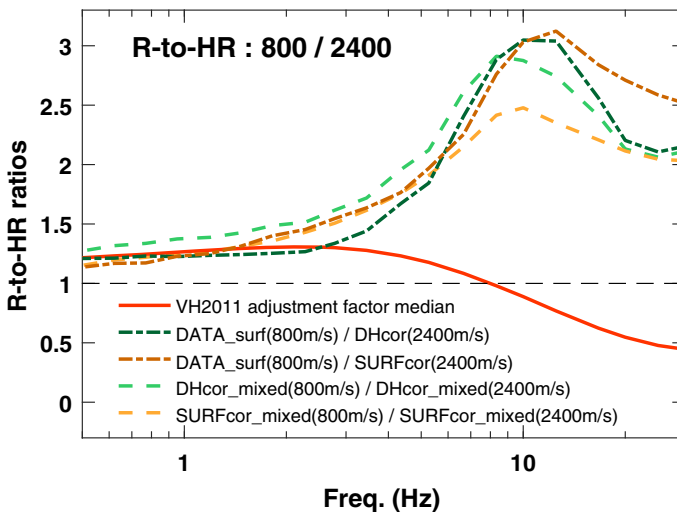


**Fig. 17** Comparison of the ratios between standard rock ( $V_S = 800$  m/s) and hard-rock ( $V_S = 2400$  m/s) obtained with the GMPEs derived in the present work (*dashed lines*), and those predicted with the H2T approach and the  $V_{S30}-\kappa_0$  approach of Van Houtte et al. (2011). The specific scenario considered here is ( $M_W = 6.5$ ;  $R_{RUP} = 20$  km), but the ratios obtained with the hybrid GMPEs (DATA\_surf + SURFcor and DATA\_surf + DHcor) are the same whatever the scenario

tests, the results are very consistent for all the GMPEs, with a significant high frequency reduction on hard rock (basically a factor 2.5–3), corresponding to the high frequency resonant amplification consistently observed at the surface of all stiff and “standard-rock” sites. On the opposite, the classical Campbell (2003) H2T approach coupled with the  $V_{S30}$ – $\kappa_0$  relationship compiled by Van Houtte et al. (2011), predicts a high frequency increase on hard-rock (by a factor about 1.25 at 10 Hz and 2 at 30 Hz), resulting from the assumed much lower  $\kappa_0$  values on very-hard rock. These large, high-frequency differences decrease progressively with decreasing frequency, to completely vanish for frequencies below 2 Hz, where all approaches predict a slightly larger motion on “standard rock” (around 20–30%). Though obtained with a completely different approach, the present results prove qualitatively consistent with the recent findings by Ktenidou and Abrahamson (2016), who analyzed a large data set including NGA-east data and others from sites with  $V_{S30} \geq 1500$  m/s, and conclude at smaller motion on hard-rock (compared to standard rock) over the whole frequency range. It must be noticed however that their ratios are closer to unity than ours, and that only few of the hard-rock sites they consider have actually measured  $V_{S30}$  values, while in our case we have the  $V_S$  profile but do not have  $\kappa_0$  values. Significant forward steps would come from datasets with many hard-rock sites with carefully measured  $V_{S30}$  and  $\kappa_0$  values.

## 6 Conclusion

The purpose of this study was to improve the understanding and the estimation of ground motion from very hard rock sites ( $1000 \leq V_S \leq 3000$  m/s) through an original processing of a subset of Japanese KiK-net recordings corresponding to stiff soils and standard rock.

Firstly, the analysis of the Japanese local site-specific responses shows that the sites with a relatively high  $V_{S30}$  ( $500 < V_{S30} < 1350$  m/s) are characterized by a significant high-frequency amplification of about 4–5 around 10 Hz in average.

Secondly, the pairs of recordings at surface and depth, together with the knowledge of the velocity profile, allow to derive different sets of “virtual” outcropping, hard-rock motion data corresponding to sites with velocities in the range [1000–3000 m/s]. The corrections are based either on a transformation of deep, within-motion to outcropping motion (DHcor), or on a deconvolution of surface recordings using the velocity profile and 1D simulation (SURFcor). Each of these virtual “outcropping hard-rock motion” data sets is then used to derive GMPEs with simple functional forms, using as site condition proxy the S-wave velocity at depth ( $V_{SDH}$ ). The predicted response spectra are finally compared with those obtained with the classical “hybrid empirical” host-to-target adjustment (H2T) approach initially proposed by Campbell (2003), coupled with the  $V_{S30}$ – $\kappa_0$  relationship compiled by Van Houtte et al. (2011). This comparison exhibits strong differences for short periods, where the H2T approach leads to predictions 3–4 times larger than the new approach presented here, in the case of hard-rock sites with  $V_{S30}$  around 2400 m/s, and a predicted  $\kappa_0$  value around 8 ms. Those differences decrease with increasing period, to completely vanish for periods exceeding 0.5 s.

The original data set (KiK-net recordings from stiff sites with  $V_{S30} \geq 500$  m/s, 1999–2009 only) is limited and has considerably enlarged over recent years. The present results should thus be considered as a first step and should be updated with an enriched dataset. However, the consistency between results obtained with completely independent correction methods (SURFcor and DHcor) allows to highlight the possible existence of a

significant bias in the classical H2T method coupled with the usually accepted  $V_{S30-\kappa_0}$  relationship, which lead to an overestimation of the hard-rock motion possibly reaching factors up to 3–4 at high frequency ( $f > 10$  Hz). Our interpretation of this bias is related to the existence of a significant, high-frequency amplification on stiff soils and standard rocks, due to thin, shallow, medium velocity layers. Not only this resonant-type amplification is not correctly accounted for by the quarter-wavelength approach used for the  $V_S$  correction factor used in the all H2T adjustment techniques, but it may also significantly impact and bias the  $\kappa$  measurements, and as a consequence the ( $V_{S30-\kappa_0}$ ) relationships implicitly used in H2T techniques.

The approaches proposed here might be applied to other strong motion datasets, provided the velocity profile is known at each recording site in order to deconvolve from the site-specific effects. This emphasizes once again the high added value of rich site metadata in all strong motion databases.

**Acknowledgements** We thank Ezio Faccioli and Philippe Renault for their help to improve the original paper. This work was carried out under the SINAPS@ project that receives French funding managed by the National Research Agency under the program “Future Investments” (Sinaps@ reference: ANR-11-RSNR-0022). Sinaps@ is a “Seism Institute” project (<http://www.institut-seism.fr/en/>). This work also benefits from previous works carried out within the frameworks of the CASHIMA program (funded by CEA, ILL and ITER) and the SIGMA program (funded by EdF, CEA, Areva and Enel). We are indebted to the National Research Institute for Earth Science and Disaster Prevention (NIED), Japan, for providing the KiK-net data and the F-NET information used for this analysis.

**Open Access** This article is distributed under the terms of the Creative Commons Attribution 4.0 International License (<http://creativecommons.org/licenses/by/4.0/>), which permits unrestricted use, distribution, and reproduction in any medium, provided you give appropriate credit to the original author(s) and the source, provide a link to the Creative Commons license, and indicate if changes were made.

## References

- Abrahamson N, Youngs R (1992) A stable algorithm for regression analyses using the random effects model. *Bull Seismol Soc Am* 82(1):505–510
- Akkar S, Sandikkaya MA, Şenyurt M, Sisi AA, Ay BÖ, Traversa P et al (2014) Reference database for seismic ground-motion in Europe (RESORCE). *Bull Earthq Eng* 12(1):311–339
- Al Atik L, Kottke A, Abrahamson N, Hollenback J (2014) Kappa ( $\kappa$ ) scaling of ground-motion prediction equations using an inverse random vibration theory approach. *Bull Seismol Soc Am* 104(1):336–346
- Ancheta TD, Darragh RB, Stewart JP, Seyhan E, Silva WJ, Chiou BSJ, Wooddel KE, Graves RW, Kottke AR, Boore DM, Kishida T, Donahue JL (2014) NGA-West2 database. *Earthq Spectra* 30(3):989–1005
- Anderson J, Hough S (1984) A model for the shape of the Fourier amplitude spectrum of acceleration at high frequencies. *Bull Seismol Soc Am* 74:1969–1993
- Aristizábal C, Bard P-Y, Beauval C, Lorito S, Selva J et al (2016) Guidelines and case studies of site monitoring to reduce the uncertainties affecting site-specific earthquake hazard assessment. Deliverable D3.4—STREST—harmonized approach to stress tests for critical infrastructures against natural hazards. <http://www.strest-eu.org/opencms/opencms/results/>. 2016. Web. 25 April 2016
- Aristizábal C, Bard P-Y, Beauval C (2017) Site-specific psha: combined effects of single station sigma, host-to-target adjustments and non-linear behavior. In: 16WCEE 2017 (16th world conference on earthquake engineering, Santiago Chile, January 9–13, 2017), paper # 1504
- Assimaki D, Li W, Steidl JH, Tsuda K (2008) Site amplification and attenuation via downhole array seismogram inversion: a comparative study of the 2003 Miyagi-Okii aftershock sequence. *Bull Seismol Soc Am* 98(1):301–330
- Bard P-Y, Gariel J-C (1986) The seismic response of two-dimensional sedimentary deposits with large vertical velocity gradients. *Bull Seismol Soc Am* 76(2):343–346
- Biro Y, Renault P (2012) Importance and impact of host-to-target conversions for ground motion prediction equations in PSHA. In: 15 WCEE, Lisboa

- Bommer JJ, Abrahamson NA (2006) Why do modern probabilistic seismic-hazard analyses often lead to increased hazard estimates? *Bull Seismol Soc Am* 96(6):1967–1977
- Bonilla LF, Steidl JH, Gariel JC, Archuleta RJ (2002) Borehole response studies at the Garner Valley downhole array, southern California. *Bull Seismol Soc Am* 92(8):3165–3179
- Boore D (2003) Simulation of ground motion using the stochastic method. *Pure Appl Geophys* 160:635–676
- Boore DM (2013) The uses and limitations of the square-root-impedance method for computing site amplification. *Bull Seismol Soc Am* 103(4):2356–2368
- Boore DM, Atkinson GM (2008) Ground-motion prediction equations for the average horizontal component of PGA, PGV, and 5%-damped PSA at spectral periods between 0.1 s and 10.0 s. *Earthq Spectra* 24(1):99–138
- Boore D, Joyner W (1997) Site amplifications for generic rock sites. *Bull Seismol Soc Am* 87:327–341
- Bora SS, Scherbaum F, Kuehn N, Stafford P, Edwards B (2015) Development of a response spectral ground-motion prediction equation (GMPE) for seismic-hazard analysis from empirical Fourier spectral and duration models. *Bull Seismol Soc Am* 105(4):2192–2218
- Bora SS, Scherbaum F, Kuehn N, Stafford P (2016) On the relationship between Fourier and response spectra: implications for the adjustment of empirical ground-motion prediction equations (GMPEs). *Bull Seismol Soc Am* 106(3):1235–1253
- Borcherdt RD (1970) Effect on local geology on ground motion near San Francisco bay. *Bull Seismol Soc Am* 60:29–61
- Brocher TM (2005) Empirical relations between elastic wavespeeds and density in the earth's crust. *Bull Seismol Soc Am* 95(6):2081–2092
- Cadet H, Bard P-Y, Rodriguez-Marek A (2010) Defining a standard rock: propositions based on the KiK-net data. *Bull Seism Soc Am* 100(1):172–195. doi:10.1785/0120090078
- Cadet H, Bard P-Y, Rodriguez-Marek A (2012) Site effect assessment using KiK-net data: part 1. A simple correction procedure for surface/downhole spectral ratios. *Bull Earthq Eng* 10(2):421–448
- Campbell KW (2003) Prediction of strong ground motion using the hybrid empirical method and its use in the development of ground-motion (attenuation) relations in eastern North America. *Bull Seismol Soc Am* 93(3):1012–1033
- Chandler AM, Lam NTK, Tsang HH (2006) Near-surface attenuation modelling based on rock shear-wave velocity profile. *Soil Dyn Earthq Eng* 26:1004–1014
- Cotton F, Scherbaum F, Bommer J, Bungum H (2006) Criteria for selecting and adjusting ground-motion models for specific target regions: application to central Europe and rock sites. *J Seismol* 10:137–156
- Cotton F, Pousse G, Bonilla F, Scherbaum F (2008) On the discrepancy of recent European ground-motion observations and predictions from empirical models: analysis of KiK-net accelerometric data and point-sources stochastic simulations. *Bull Seismol Soc Am* 98(5):2244
- Douglas J, Gehl P, Bonilla LF, Gélis C (2010) A  $\kappa$  model for mainland France. *Pure Appl Geophys* 167(11):1303–1315
- Drouet S, Cotton F, Gueguen P (2010)  $V_{S30}$ ,  $\kappa$ , regional attenuation and Mw from accelerograms: application to magnitude 3–5 French earthquakes. *Geophys J Int* 182(2):880–898
- Edwards B, Faeh D, Giardini D (2011) Attenuation of seismic shear-wave energy in Switzerland. *Geophys J Int* 185:967–984
- Fujiwara H, Aoi S, Kunugi T, Adachi S (2004) Strong-motion observations of NIED: K-NET and KiK-net. In: Proceedings of the COSMOS workshop on record processing guidelines
- Fukushima Y, Gariel JC, Tanaka R (1995) Site-dependent attenuation relations of seismic motion parameters at depth using borehole data. *Bull Seismol Soc Am* 85(6):1790–1804
- Hollender F, Foundotos L, Laurendeau A, Bard P-Y, Hernandez B, Drouet S, Ktenidou OJ, Perron V, Letort J (2015) Correction of surface records of their site effect before developing GMPE: an alternative approach to get reference incident ground motion (application to KiK-net data). In: SIGMA/SINAPS@ report ref. SINAPS@-2015-V1-A1-T3-1, June 2015
- Hough SE, Anderson JG (1988) High-frequency spectra observed at Anza, California: implications for Q structure. *Bull Seismol Soc Am* 78:692–707
- Joyner WB, Warrick RE, Fumal TE (1981) The effect of Quaternary alluvium on strong ground motion in the Coyote Lake, California, earthquake of 1979. *Bull Seismol Soc Am* 71(4):1333–1349
- Kanno T, Narita A, Morikawa N, Fujiwara H, Fukushima Y (2006) A new attenuation relation for strong ground motion in Japan based on recorded data. *Bull Seismol Soc Am* 96(3):879–897
- Kennett BLN (1974) Reflections, rays, and reverberations. *Bull Seismol Soc Am* 64(6):1685–1696
- Kinoshita S (1998) Kyoshin net (K-NET). *Seismol Res Lett* 69(4):309–332
- Kishida T, Ktenidou OJ, Darragh RB, Walter S (2016) Semi-automated procedure for windowing time series and computing Fourier amplitude spectra (FAS) for the NGA-West2 database. PEER report no. 2016/02

- Konno K, Ohmachi T (1998) Ground-motion characteristics estimated from spectral ratio between horizontal and vertical components of microtremor. *Bull Seismol Soc Am* 88(1):228–241
- Kottke AR (2017)  $V_{S30}$ - $\kappa_0$  relationship implied by ground motion models? In: 16WCEE 2017 (16th world conference on earthquake engineering, Santiago Chile, January 9–13, 2017), paper # 3089
- Ktenidou OJ, Abrahamson NA (2016) Empirical estimation of high-frequency ground motion on hard rock. *Seismol Res Lett* 87(6):1465–1478
- Ktenidou O-J, Cotton F, Abrahamson NA, Anderson JG (2014) Taxonomy of  $\kappa$ : a review of definitions and estimation approaches targeted to applications. *Seismol Res Lett* 85:135–146
- Ktenidou OJ, Abrahamson NA, Drouet S, Cotton F (2015) Understanding the physics of kappa ( $\kappa$ ): insights from a downhole array. *Geophys J Int* 203(1):678–691
- Laurendeau A, Cotton F, Ktenidou O-J, Bonilla L-F, Hollender F (2013) Rock and stiff-soil site amplification: dependency on  $V_{S30}$  and kappa ( $\kappa_0$ ). *Bull Seismol Soc Am* 103(6):3131–3148
- Laurendeau A, Bard P-Y, Hollender F, Ktedinou OJ, Foundotos L, Hernandez B, Perron V (2016) Prediction of reference motions ( $1000 < V_s < 3000$  m/s) from corrected KiK-net records of the local site effects. In: 5th IASPEI/IAEE international symposium: effects of surface geology on seismic motion, August 15–17, Taipei
- Lebrun B, Hatzfeld D, Bard P-Y (2001) A site effect study in urban area: experimental results in Grenoble (France). *Pure Appl Geophys* 158:2543–2557
- Lermo J, Chavez-Garcia FJ (1993) Site effect evaluation using spectral ratios with only one station. *Bull Seismol Soc Am* 83(5):1574–1594
- Maufroy E, Chaljub E, Hollender F, Kristek J, Moczo P, Klin P, De Martin F (2015) Earthquake ground motion in the Mygdonian Basin, Greece: the E2VP verification and validation of 3D numerical simulation up to 4 Hz. *Bull Seismol Soc Am* 105:1398–1418. doi:[10.1785/0120140228](https://doi.org/10.1785/0120140228)
- Maufroy E, Chaljub E, Theodoulidis N, Roumelioti Z, Hollender F, Bard P-Y, De Martin F, Guyonnet-Benaize C, Margerin L (2017) Source-related variability of site response in the Mygdonian basin (Greece) from accelerometric recordings and 3-D numerical simulations. *BSSA*. doi:[10.1785/0120160107](https://doi.org/10.1785/0120160107)
- Okada Y, Kasahara K, Hori S, Obara K, Sekiguchi S, Fujiwara H, Yamamoto A (2004) Recent progress of seismic observation networks in Japan—Hi-net, F-net, K-NET and KiK-net. *Earth Planets Space* 56:xv–xxviii
- Olsen K, Day S, Bradley C (2003) Estimation of Q for long-period (>2 sec) waves in the Los Angeles basin. *Bull Seismol Soc Am* 93:627–638
- Parolai S, Bindi D (2004) Influence of soil-layer properties on k evaluation. *Bull Seismol Soc Am* 94(1):349–356
- Perron V, Laurendeau A, Hollender F, Bard P-Y, Gélis C, Traversa P (2017) Selecting time windows of seismic phases and noise for engineering seismology applications: a versatile methodology and algorithm. *Bull Earthq Eng*. doi:[10.1007/s10518-017-0131-9](https://doi.org/10.1007/s10518-017-0131-9)
- Pilz M, Fäh D (2017) The contribution of scattering to near-surface attenuation. *J Seismol* 1–19. doi:[10.1007/s10950-017-9638-4](https://doi.org/10.1007/s10950-017-9638-4)
- Poggi V, Edwards B, Fäh D (2013) Reference S-wave velocity profile and attenuation models for ground-motion prediction equations: application to Japan. *Bull Seismol Soc Am* 103(5):2645–2656
- Rodriguez-Marek A, Montalva GA, Cotton F, Bonilla F (2011) Analysis of single-station standard deviation using the KiK-net data. *Bull Seismol Soc Am* 101(3):1242–1258
- Rodriguez-Marek A, Rathje EM, Bommer JJ, Scherbaum F, Stafford PJ (2014) Application of single-station sigma and site-response characterization in a probabilistic seismic-hazard analysis for a new nuclear site. *Bull Seismol Soc Am* 104:1601–1619
- Silva W, Darragh RB, Gregor N, Martin G, Abrahamson N, Kircher C (1998) Reassessment of site coefficients and near-fault factors for building code provisions. Technical report program element II: 98-HQ-GR-1010, Pacific Engineering and Analysis, El Cerrito
- Steidl JH, Tumarkin AG, Archuleta RJ (1996) What is a reference site? *Bull Seismol Soc Am* 86(6):1733–1748
- Theodoulidis N, Bard P-Y (1995) Horizontal to vertical spectral ratio and geological conditions—an analysis of strong ground motion data from Greece and Taiwan (smart-1). *Soil Dyn Earthq Eng* 14(3):177–197
- Thompson EM, Baise LG, Tanaka Y, Kayen RE (2012) A taxonomy of site response complexity. *Soil Dyn Earthq Eng* 41:32–43
- Tumarkin AG, Archuleta RJ (1992) Parametric models of spectra for ground motion prediction. *Seismol Res Lett* 69:30
- Van Houtte C, Drouet S, Cotton F (2011) Analysis of the origins of  $\kappa$  (kappa) to compute hard rock to rock adjustment factors for GMPEs. *Bull Seismol Soc Am* 101(6):2926–2941